Chapter 5

As-Cast Microstructure, Texture and Properties

5.1 Introduction

An important metallurgical challenge associated with the development of direct strip casting is the need to reassess our understanding of the relationship between microstructure and properties. The casting processes involved are usually characterised by high solidification rates which often produce far-from-equilibrium microstructures. This chapter provides an overview of the factors affecting the microstructure, texture and properties in various commercially-significant alloys produced by DSC. The various methods of representing textures are outlined in Appendix B.

~~5.2 General features of strip-cast microstructures~~

~~5.2.1 Dendritic growth in a flowing melt~~

~~The heat flow in DSC is often highly directional with the maximum interfacial heat flux occurring perpendicular to the wall of the mould (§4.5). In the absence of inoculation, the heat flow conditions favour the formation of columnar grains in as-cast strip. In twin belt and twin roll casting, a solidifying shell is produced at each mould surface; these shells coarsen by dendritic growth and eventually interact to produce the as-solidified strip (Figure 4.12). Under certain casting conditions, a central equiaxed zone may also develop which separates these columnar regions.~~

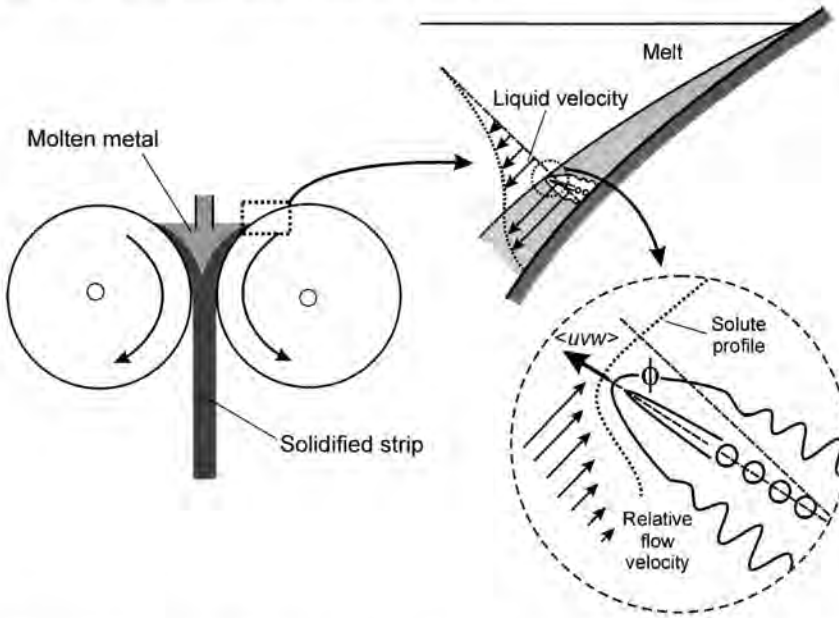

Figure 5.1. Schematic diagram showing the influence of a flowing melt on dendrite growth behaviour in twin roll casting, after Takatani *et al.* (2000) (with kind permission of Elsevier Limited).

It was shown in Table 2.2 that casting results in the growth of dendrites parallel to certain crystallographic directions. In both pure and impure materials, flow of liquid metal parallel to the mould wall results in the deviation of the preferred growth direction of dendrites away from the maximum heat flux direction (§2.3.3.2). This is significant as the movement of the mould wall/s relative to the melt pool is a characteristic feature of all moving mould casting processes. Figure 5.1 shows schematically the solidification of strip on the counter-rotating rolls of a twin roll caster and the formation of a thin solid shell on one of the rolls with subsequent growth of dendrites at an angle (ϕ) towards the casting direction (CD) (inset). It is important to note that since both the liquid and mould are moving, the velocity of the melt *relative* to the growing dendrites (which are moving at the same speed as the rolls) affects the degree of inclination of the dendrites.

The effect of mould/substrate velocity on the deflection angle, ϕ, of dendrites is given in Figure 5.2 for a range of alloys and casting processes. While there is some scatter of the data, it is clear that casting velocity has a substantial impact on dendritic growth which, in turn, affects the final microstructure and texture of the strip. The scatter in the data is probably due to the nature of the various casting processes where the actual velocity of the melt *relative* to the growing dendrites is not known accurately. Other important factors include melt

conditions, alloy type and the concentration of alloying elements. For example, alloying elements influence the growth direction of dendrites relative to a flowing melt by generating an asymmetrical solute field at the dendrite tip (§2.3.3.2). Esaka and co-workers (1996) have demonstrated the effect of carbon concentration in molten iron on ϕ for the situation where the melt is flowing down an inclined plane. These workers derived the following empirical relation for alloys containing carbon contents, C_o, in the range 0.005 to 1.0 wt.%:

$$\phi = \log\left(\frac{0.538 v_F^{2.08}}{R}\right)\cdot\left(\frac{0.35 C_o^2}{C_o^2 + 0.0005} + 0.65\right)\cdot 11.5 v_F^{-0.177} \qquad (5.1)$$

For a given flow velocity (governed by the angle of inclination of the substrate) and solidification rate, Eq. 5.2 predicts that an increase in carbon content will result in a small increase in ϕ.

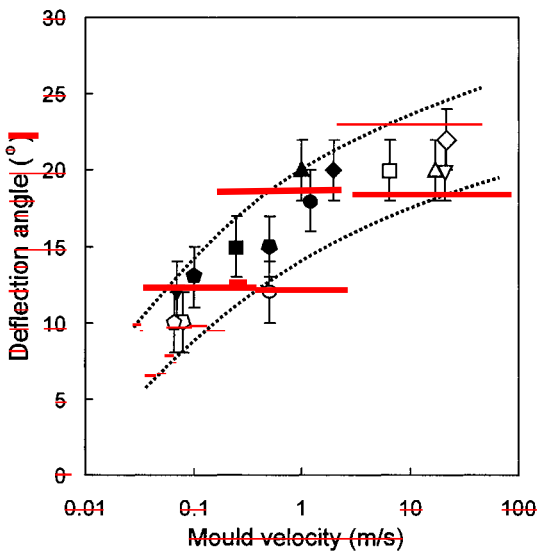

	Alloy	Process	Source		Alloy	Process	Source
■	Fe-3Si	TRC	Takatani *et al.* (2000)	○	Fe-C alloys	TSC	Ushijima *et al.* (1987)
□	Fe-4Si	TRC	Zapuskalov (1996)	▲	Fe-(0.05-1.0)C	Inclined plane	Esaka *et al.* (1996)
◆	Fe-3.5Si	TRC	Reszetko & Bigot (1992)	△	Fe-20Cr-5Al-La	CBMS	Lee *et al.* (1996)
◇	Fe-6.5Si	CBMS	Jang *et al.* (1992)	▬	HSLA-80 steel	Single Belt	Krishnadev *et al.* (1992)
●	AISI 304 (SS)	TRC	Takuda *et al.* (1991)	○	Cu-Sn-Ni	Stationary	Es-Sadiqi *et al.* (1989)
○	AISI 304 (SS)	Dipping	Lee (2002)	▼	AZ91 (Mg)	TRC	Park *et al.* (2003)
▬	AISI 304 (SS)	SRC	Grubb *et al.* (1987)	▽	Pd-2.8Ni	CBMS	Thoma *et al.* (1996)

Figure 5.2. Effect of mould velocity on the average deflection angle of dendrites in solidified samples for a range of alloys and casting processes (due to rolling effects, see §5.4.1.2, the data excludes Al alloys).

Table 5.1. Effect of cooling rate during casting on secondary dendrite arm spacing for some alloys. [data based on $\lambda_2 = a\dot{T}^{-n}$ (Eq. 2.37)]

Material	Source	Cooling rate range (K/s)	$\bar{a}$	$\bar{n}$
Fe-(0.1-0.9%C) steels	Suzuki *et al.* (1968)	$\dot{T} = 3\times10^{-2} - 1.7\times10^{1}$	158	0.36
Fe-25%Ni alloy	Flemings *et al.* (1970)	$\dot{T} = 10^{-3} - 10^{1}$	84	0.27
AISI 304 stainless steel	Sugiyama *et al.* (1974)	$\dot{T} = 10^{2} - 10^{3}$	62	0.47
AISI 304 stainless steel	Wolf (1986)	$\dot{T} = 6\times10^{0} - 1.45\times10^{3}$	82	0.30
AISI 304 stainless steel	Esaka *et al.* (1988)	$\dot{T} = 2\times10^{-1} - 10^{3}$	111	0.45
AISI 304 stainless steel	Gunji *et al.* (1989)	$\dot{T} = 10^{-2} - 10^{3}$	96	0.25
AISI 304 stainless steel	Mizukami *et al.* (1992)	$\dot{T} = 10^{-1} - 10^{4}$	100	0.35
Cu-2.3%Sn-9.5%Ni alloy	Es-Sadiqi *et al.* (1989)	$\dot{T} = 10^{2} - 10^{3}$	100	0.35
Aluminium casting alloys	Spear and Gardner (1963)	$\dot{T} = 10^{-1} - 10^{2}$	46	0.33
Al-(0.25-0.55%Fe) alloys	Miki *et al.* (1975)	$\dot{T} = 10^{-2} - 4.2\times10^{1}$	33	0.33
Al-4.5%Cu alloy	Munitz (1985)	$\dot{T} = 10^{-4} - 10^{7}$	45	0.33
Al-9%Si-3%Cu-2%Zn alloy	Es-Sadiqi *et al.* (1988)	$\dot{T} = 10^{2} - 10^{3}$	38	0.43
Al-Mn & Al-Cu-Mn alloys	Merchant *et al.* (1989)	$\dot{T} = 10^{-3} - 10^{4}$	40	0.27

5.2.2 Secondary dendrite arm spacing

The secondary dendrite arm spacing (SDAS) of alloys is often described by a relationship of the form $\lambda_2 = a\dot{T}^{-n}$ (Eq. 2.37). The effect of cooling rate on SDAS has been investigated for a wide range of casting processes and Table 5.1 shows data for some important ferrous and non-ferrous alloys. These data are plotted in Figure 5.3 showing the range of cooling rates expected for a particular casting process. For each class of alloy, the data fall in a band with n values of all alloys ranging from 0.25 to 0.5 which encompasses theoretical prediction (Eq. 2.36). For a given cooling rate, steels solidify with the largest dendrite spacing whereas Al alloys develop a finer microstructure. These differences arise probably because SDAS varies with time during solidification due to growth and coarsening of the dendrite arms which is affected by the concentration and diffusivity of solute elements in both the liquid and solid states (§2.3.2.1). Nevertheless, the simple relationships shown in Figure 5.3 are useful for estimating the cooling rates in various casting processes, and particularly strip casting where cooling rates over 100 K/s are very difficult to measure.

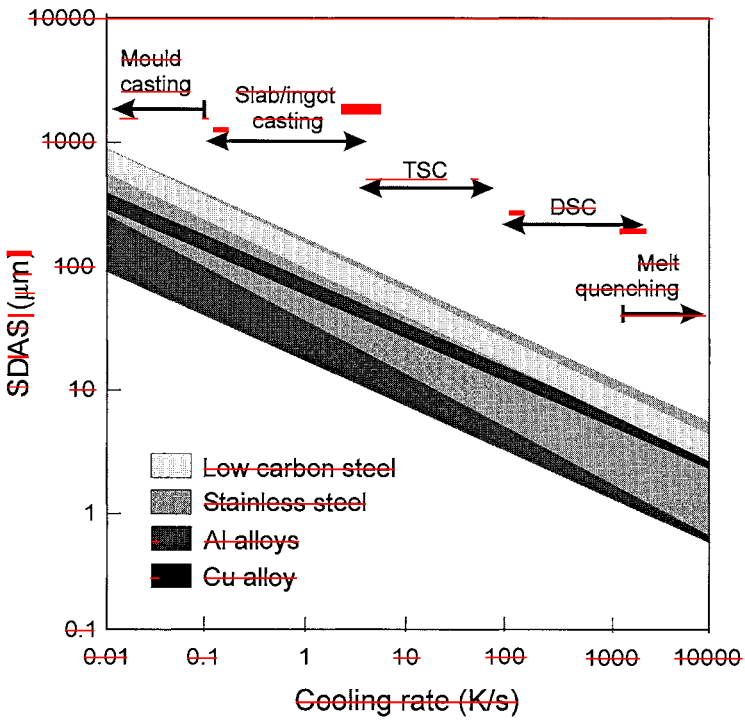

Figure 5.3. Summary of the influence of cooling rate on SDAS for a range of alloys and casting processes (data plotted from Table 5.1).

5.3 Strip-cast ferrous alloys

Direct strip casting of iron alloys is carried out by the twin roll process (§3.2.3) although belt and stationary mold casters can be used to make thicker gauge strip (§3.2.2). In TRC, the strip is cast through water-cooled copper rolls with the force exerted on the solidifying shells not sufficiently large to impart any substantial reduction of the strip (§4.4.2). The alloys most amenable to TRC are stainless steels, carbon steels and silicon iron. These alloys have reached the commercial stage of production although other steels are under investigation.

5.3.1 Low carbon steels

Low carbon steels are a class of alloys with carbon levels below 0.2% but generally containing various other elements (§1.2.3.1). The ability to produce low carbon steel by DSC has been one of the biggest recent challenges facing the metallurgical industry but TRC of low carbon steel is now a commercial reality (§3.2.2.1). Hence, the as-cast structure and properties of this class of steel have been the subject of considerable ongoing and often highly confidential research. The following sections outline the current status of microstructural development of low carbon steel, as obtained from the open literature.

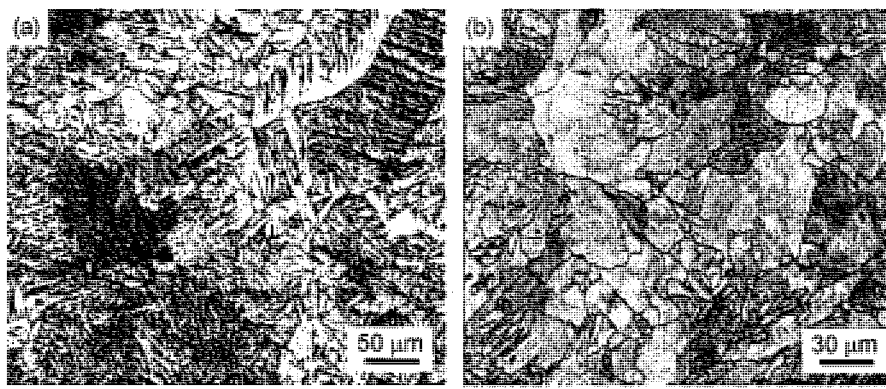

Figure 5.4. Typical as-cast microstructure in strip-cast low carbon steel: (a) optical micrograph, and (b) EBSD micrograph, courtesy of W. Xu.

5.3.1.1 As-cast microstructure

One of the first published researches on the microstructural development of strip-cast low carbon steel was carried out by Shiang and Wray (1989). Their Al-killed 0.05 wt.% C steel was cast by TRC to a thickness of 1.5-2.2 mm at a casting speed of 0.5 m/s which equates to a solidification rate in the range 10^2 to 10^4 K/s at the strip surface (Figure 4.22). The microstructure was reported to

consist mainly of Widmanstätten ferrite, polygonal ferrite, pearlite and grain boundary carbides; this microstructure is markedly different to that of CCC slab. The non-equilibrium microstructure was believed to be the result of the development of coarse columnar austenite grains (~250 μm in width) during casting, together with the relatively rapid cooling rate and chemical composition of the steel.

Typical strip-cast microstructures of C-Mn steel produced by TRC are shown in Figure 5.4. Figure 5.4a is an optical micrograph showing Widmanstätten and acicular ferrite and, to a lesser degree, pearlite, with some polygonal ferrite developing at the strip surfaces (not shown). The distribution in grain orientations is given in the EBSD micrograph of Figure 5.4b where a given orientation (grain) is shown as a particular grey-scale. The coarser polygonal-shaped grains contain an internal substructure, as indicated by the variation in grey-scale within these grains. The mixed microstructure of strip-cast material is very similar to that produced in C-Mn weld deposits (Bhadeshia and Svensson 1993) which is to be expected since both solidification reactions generate coarse austenite grains and involve rapid cooling rates through the critical transformation temperature range. Figure 5.5 shows, for welds produced using C-Mn steel, the variation in microstructure in the weld metal zone as a function of carbon content. For a carbon content of 0.06% (dashed line), the type and volume fraction of phases produced by welding are similar to that found in an equivalent grade of steel produced by TRC (Figure 5.4a). This behaviour is expected since both types of microstructure are the product of rapid solidification.

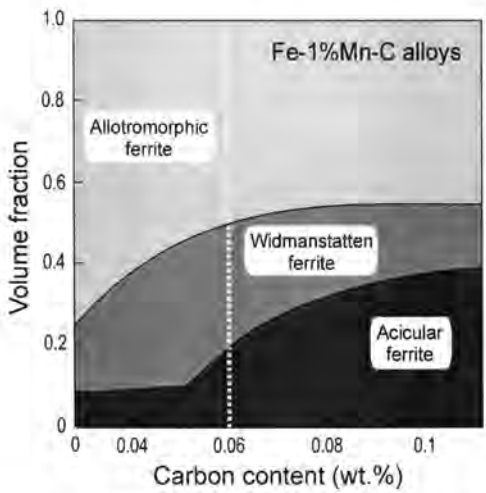

Figure 5.5. The variation in microstructure as a function of carbon content in C-Mn steel weld deposits, after Bhadeshia and Svensson (1993) (with kind permission of The Institute of Materials, Minerals and Mining, UK).

The formation of Widmanstätten ferrite and other non-equilibrium phases during strip casting is attributed to the coarse prior austenite grain size produced during solidification and the rapid cooling through the critical temperature range of austenite decomposition (Aaronson 1962). In this situation, normal polygonal growth of ferrite is unable to keep up with the rate of decrease in temperature and the plate-like ferrite morphology shown in Figure 5.4a is developed via nucleation either at austenite grain boundaries (Widmanstätten ferrite) or intragranular sites (acicular ferrite). Due to crystallographic considerations, these types of ferrite grow rapidly by the lateral movement of ledges along low-energy γ / α interfaces (Bhadeshia 2001).

The microstructure and mechanical properties of low carbon steel strip produced by direct casting and CCC/TMP are summarised in Table 5.2. It is clear that these processes produce markedly different austenite and ferrite microstructures and that the volume fraction of each type of ferrite generated by strip casting is in accordance with that produced in weld deposits (Figure 5.5). The fine, equiaxed ferrite microstructure produced by conventional processing is well-understood and is a result of the large reductions used which break up the original cast structure leading to a significant refinement of austenite. Further transformation produces the fine ferrite microstructure (Ray *et al.* 1994; Humphreys and Hatherly 2004). There is also a marked dendrite refinement in strip-cast material compared with CCC which is expected to strongly influence the rate of homogenisation if this type of heat treatment is part of the downstream processing stage (§6.3.2.2).

Table 5.2. Microstructures and properties of strip-cast and CCC/TMP-produced low carbon steel, adapted from Mukunthan *et al.* (2000).

Feature/ property	Strip casting	Hot strip mill
Prior austenite grain morphology, size	Columnar shape 100 to 250 μm in width 300 to 700 μm in length	Equiaxed 25 μm
Final microstructure constituents	30 to 60% polygonal ferrite 70 to 40% Widmanstätten and acicular ferrite	100% equiaxed ferrite
Ferrite grain morphology, size	Polygonal: 10 to 50 μm in width and 50 to 250 μm in length	Equiaxed 10 μm
SDAS	5 to 15 μm	100 to 250 μm (CCC)
Final texture	Weak	Varies depending on TMP conditions*
Yield strength	280 to 340 MPa	250 to 320 MPa
Tensile elongation	20 to 30%	28 to 36%

* Ray and Jonas (1990), Ray *et al.* (1994).

When strip casting is carried out using water-cooled rolls or belts, it is generally observed that the dendrite arm spacing increases with distance from the strip surface which indicates a decrease in cooling rate into the core of the strip (see *e.g.* Figure 5.6). Using the data of Suzuki *et al.* (1968) in Table 5.1, cooling rates associated with TRC range from 10^4K/s to 6×10^4K/s at the surface and core, respectively. An interesting aspect of Figure 5.6 is the finer dendrite arm spacing for a given distance below the strip surface in TRC compared with single-roll casting. This implies that a higher cooling rate is generated at an equivalent distance from the solidifying surface in the TRC process but reasons for such a difference were not given.

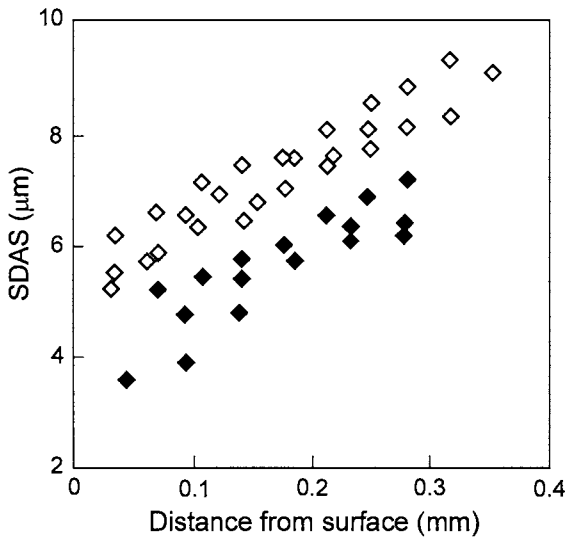

Figure 5.6. SDAS as a function of distance from the strip surface of low carbon steel produced by single roll casting (open symbols) and twin roll casting (filled symbols), after Cramb (1995) (with kind permission of CIMMP, Canada).

It was shown in Figure 5.2 that, for a given cooling rate, SDAS depends on the type of alloy being cast. For example, low carbon steels generate a coarser dendrite arm spacing compared with the more highly alloyed stainless steels. Cabrera-Marrero and co-workers (1998) have shown that both the primary and secondary dendrite arm spacing in a range of carbon steels follow relationships of the form of Eqs 2.35 (λ_1) and 2.36 (λ_2). Figure 5.7 illustrates the close correlation between these equations and the data for Fe-0.08C-1.48Mn-0.86Si alloy produced by thin slab casting. For a wide range of carbon steels, these workers demonstrated that both λ_1 and λ_2 are related to the alloying elements in the melt and proposed the following relationships:

$$\lambda_1 = \frac{1}{R^{1/4}G^{1/2}}[1990\%C + 380\%Si - 0.221\%Mn - 9840\%Al + 20\%Ni - 40\%Cr] \quad (5.2)$$

$$\lambda_2 = t_f^{1/3}[70\%C + 50\%Si - 1.78\%Mn - 430\%Al + 0.755\%Ni - 3.42\%Cr] \quad (5.3)$$

where R is in cm/s, G in K/cm, $t_f^{1/3}$ in seconds and λ_1 and λ_2 in μm. It can be seen that λ_2 increases with increasing C, Si and Ni contents but decreases for increasing Mn, Al and Cr contents.

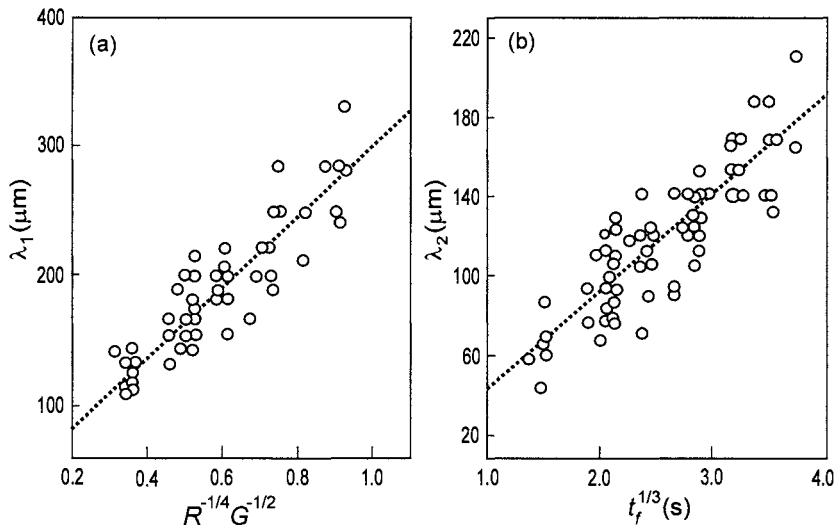

Figure 5.7. Effect of casting variables based on Eqs. 2.35 and 2.36 on: (a) primary dendrite and (b) secondary dendrite arm spacing for an as-cast Fe-0.08%C-1.48%Mn-0.86%Si steel, after Cabrera-Marrero *et al.* (1998) (with kind permission of The Iron and Steel Institute of Japan).

Despite the markedly different microstructures produced by TRC compared with conventional processing, there is only a small increase in strength and decrease in ductility in the as-cast strip (Table 5.2). Honeycombe and Bhadeshia (1995) reported the major factors contributing to the strength of low carbon steels to be: (i) solid solution strengthening by interstitial and substitutional atoms; (ii) grain size strengthening; (iii) dispersion strengthening, and (iv) dislocation strengthening. Table 5.2 shows that the differences in mechanical properties are not large but the slightly higher strength in as-cast strip is likely to be associated with higher dislocation content of Widmanstätten and acicular ferrite (Couture *et al.* 1992; Ferry and Page 2001) together with some degree of solid solution strengthening from elements such as C, Mn and Si due to the high cooling rates generated by casting.

5.3.1.2 As-cast texture

Solidification of low carbon steel during strip casting commences by the nucleation of delta-ferrite at the meniscus (mould/liquid interface). The heat flow conditions favour the formation of a dendritic delta-ferrite structure that subsequently transforms to austenite to produce columnar grains of width governed by casting variables and steel composition (Mukunthan *et al.* 2000). Further cooling resulting in the final transformation to various decomposition products, as described in §1.2.3.1. The successive transformations: $\delta \rightarrow \gamma \rightarrow \alpha$ have a marked influence on the final texture of the strip (Okamoto 1988; Couture *et al.* 1992; Girgensohn *et al.* 2000; Cramb and Rollett 2001).

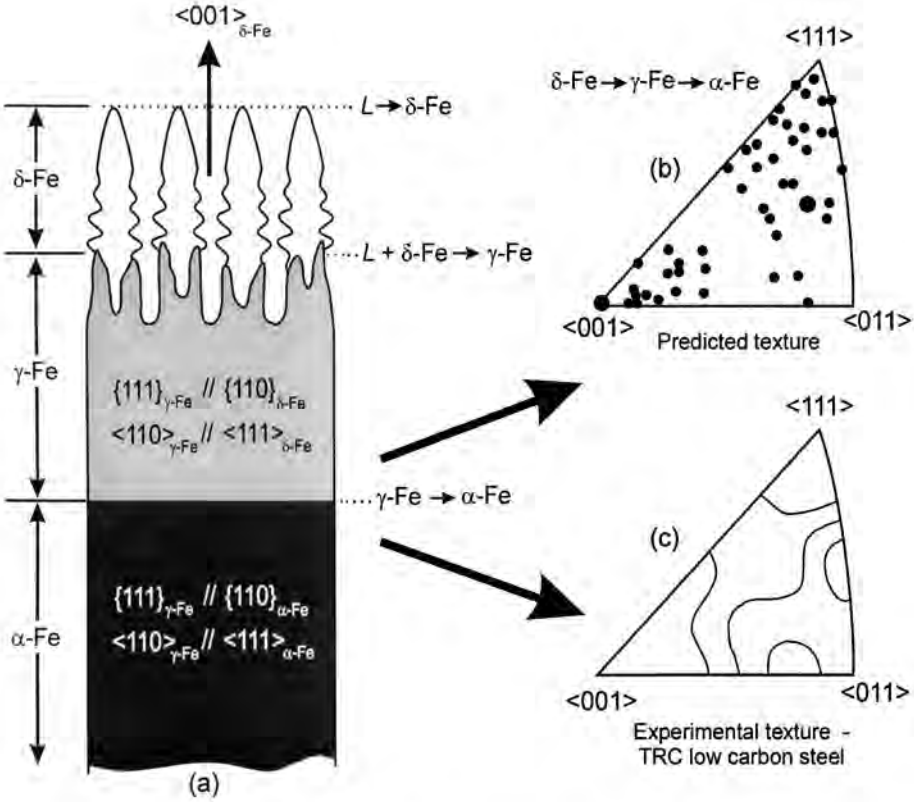

Figure 5.8. Schematic diagram showing the transformation sequence during dendritic solidification of low carbon steel, adapted from Kluken *et al.* (1991). (b) Inverse pole figure of the texture expected from a <001> oriented grain of delta-ferrite after transformation through to ferrite, adapted from Okamoto (1988). (c) Experimental inverse pole figure of twin roll cast low carbon steel, courtesy of W. Xu.

Figure 5.8 is a schematic diagram showing dendritic growth of delta-ferrite and the subsequent transformations to austenite and acicular or Widmanstätten ferrite. It is possible to understand the origin of the final texture in low carbon steel if it assumed that an initial <001>-oriented delta-ferrite grain transforms to austenite which in turn transforms to ferrite in accordance with the Kurdjumov-Sachs (K-S) orientation relationship (Bunge 1982). The K-S relationship is observed in diffusional transformations of a range of cubic alloys where the parent phase transforms to produce up to 24 crystallographic variants of the product phase by the following relation:

$$\{111\}_{fcc} // \{011\}_{bcc}$$
$$<0\bar{1}1>_{fcc} // <1\bar{1}1>_{bcc}$$

During the dendritic growth of delta-ferrite into the melt, nucleation of austenite occurs by the peritectic reaction behind the solidification front. The austenite subsequently grows and consumes the primary phase with impingement occurring on neighbouring columnar grain boundaries. If the cooling rate through the critical temperature range is high, the coarse austenite grains subsequently transform to either Widmanstätten or acicular ferrite. Assuming that all 24 variants of the K-S relationship are equally expected, the inverse pole figure of the final texture after austenite transforms to these types of ferrite is given in Figure 5.8b. An experimental inverse pole figure of C-Mn low carbon steel produced by TRC is shown for comparison in Figure 5.8c. The weak texture in Figure 5.8c is expected due to the multiplicity of orientations generated by decomposition of austenite to ferrite but is slightly weaker than that predicted in Figure 5.8b since the final texture is the average of a large number of differently oriented austenite grains.

5.3.1.3 Methods of modifying the as-cast microstructure

Although the rapid cooling rates associated with direct mould/metal contact and air cooling of strip-cast low carbon steel promote the formation of non-equilibrium microstructures, certain alloying additions and the control of nucleation sites during solidification can result in substantial austenite refinement. This allows the possibility of modifying acicular/Widmanstätten ferrite to a more polygonal morphology (Mukunthan *et al.* 2000).

It is known that tellurium, sulphur and other additions to molten steel decrease the melt/substrate surface tension (for a smooth substrate surface) which results in an increase in heat flux during the initial stages of solidification (see §4.5.3.4). The overall effect is an increase in the nucleation efficiency of delta-ferrite which subsequently refines the austenite grain width (Mukunthan *et al.* 2000). It was shown in §4.5.3 that interfacial heat flux during solidification can be controlled directly by substrate topography (by machining ridges in the mould surface to promote nucleation along their peaks). The effect of these variables

on austenite grain refinement is summarised in Figure 5.9 where it can be seen that sulphur content in combination with a textured substrate reduces the austenite grain width by over 50-80%. Both factors have a significant influence on the final ferrite morphology by altering the transformation path of the steel to generate 100% polygonal ferrite (Mukunthan *et al.* 2000).

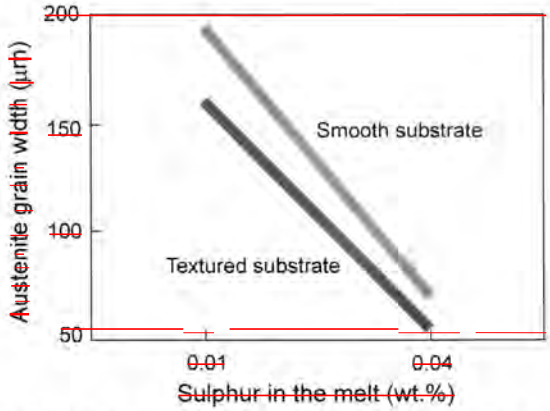

Figure 5.9. Influence of sulphur and substrate topography on austenite grain width in strip-cast low carbon steel, adapted from Mukunthan *et al.* (2000).

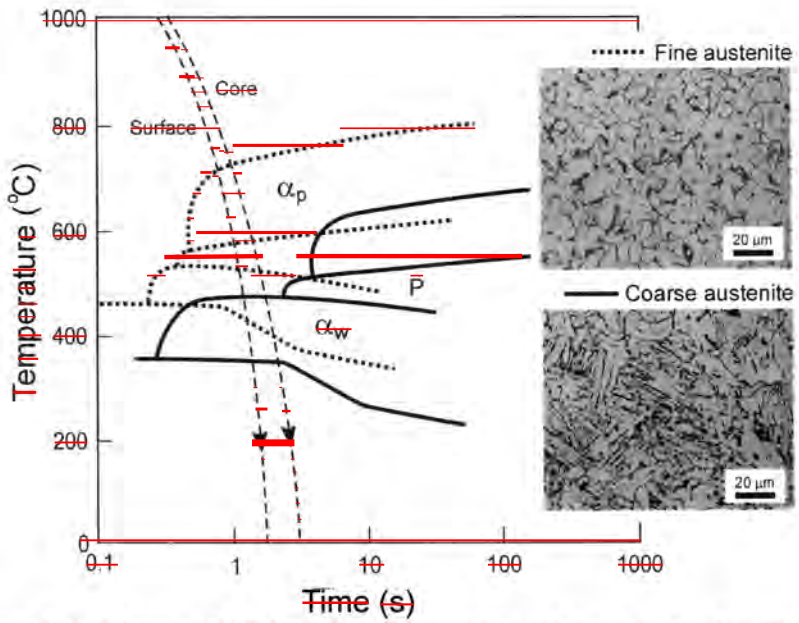

Figure 5.10. Schematic CCT diagram for low carbon steel showing the effect of austenite grain size on the mode of austenite decomposition.

~~The influence of austenite grain size (width) on the mode of austenite decomposition in low carbon steel is shown in the schematic continuous cooling transformation (CCT) diagram in Figure 5.10. Superimposed on the diagram are the cooling curves expected in both the surface and core of 1 mm gauge strip as it solidifies during twin roll casting. This figure shows that a decrease in the austenite grain width changes ferrite from Widmanstätten/acicular to mainly polygonal.~~

~~In addition to the control of solidification conditions and alloying additions in low carbon steel, there is considerable scope for further modification of the as-cast structure by controlled cooling and elevated temperature coiling (§6.3.1), conventional hot rolling (§6.4.1), in-line hot rolling (§6.4.2), and re-austenitisation (§6.3.2.1) and cold rolling and annealing (§6.6.3.1)~~

5.3.2 Austenitic stainless steels

Austenitic stainless steels contain high Cr and Ni levels (§1.2.3.2). There is considerable interest in DSC of these types of steel since it is anticipated that they will be produced in large tonnages by this process. The solidification sequence of stainless steel is dependent both on alloying additions and solidification rate with the $(Cr/Ni)_{eq}$ ratio shown to be an important parameter (§1.2.3.2).

5.3.2.1 As-cast grain structure

In TRC of austenitic stainless steel, the two shells that form on each roll often exhibit a columnar structure with the grains inclined in the direction of casting (Figure 5.1). Under certain circumstances a central equiaxed zone will form in the strip and is argued to form by various mechanisms (see Mizoguchi and Miyazawa 1995). These workers carried out a detailed analysis of the influence of casting variables on the microstructural development of AISI 304 by twin roll casting. It was found, for a high melt superheat, that an increase in the roll gap produced a substantial increase in the width of this zone. This was attributed to the incomplete impingement of the growing shells as they pass through the rolls of the strip caster with the remaining liquid in the core of the strip solidifying by the preferential growth of free crystallites ahead of the solidification front. An abrupt decrease in interfacial heat flux is also expected as the strip passes through the roll nip (Figure 4.29) and will reduce the directionality of heat flow to favour equiaxed solidification rather than further columnar growth.

Similar to low carbon steel, the secondary dendrite arm spacing in twin roll cast AISI 304 stainless steel is a strong function of cooling rate (Figure 5.2) and also increases with distance from the strip surface, Figure 5.11. There is also a significant influence of mould material on this parameter with cooling rates,

estimated using Mizukami's relation (Mizukami *et al.* 1992), of 5×10^3-5×10^2 K/s (steel rolls) and 9×10^3-5×10^3 K/s (copper rolls), respectively.

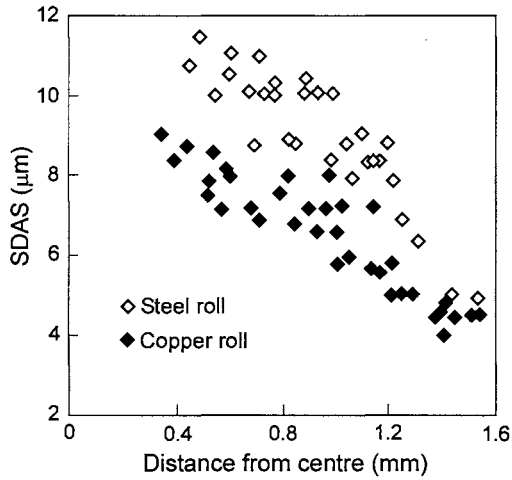

Figure 5.11. SDAS as a function of distance from the as-cast surface of twin roll cast AISI 304 showing the effect of roll material on structural refinement, after Jeong *et al.* (1999).

A systematic study of the influence of casting variables on microstructural development in AISI 304 was carried out by Strezov and co-workers using the strip casting simulator described in §A.2.2. Figure 5.12 shows the influence of interfacial heat flux on the rate of surface nucleation in AISI 304 for both smooth and ridged copper substrates (see *e.g.* Figure A.2). The increase in maximum heat flux in Figure 5.12 was achieved by improving the contact effectiveness at the meniscus by adding sulphur to the melt or increasing casting velocity etc (see §4.5.3). For a ridged substrate, the effect of heat flux on nucleation rate is marginal whereas, for the smooth substrate, there is substantial increase in nucleation density with increasing heat flux.

The data in Figure 5.12 show that a textured (ridged) substrate almost completely dominates the nucleation behaviour regardless of changes in heat flux. In this situation, interfacial heat flux is spatially variable with a high flux through the peaks of the ridges accompanied by extremely high cooling rates to promote nucleation along the peaks (Strezov and Herbertson 1998). Figure 5.13a is a schematic diagram of the local variation in heat flux transverse to a row of ridges on a ridged substrate. An EBSD micrograph of the preferred nucleation along the ridges is given in Figure 5.13b. Overall, machining ridges onto the mould surface produces a consistent nucleation pattern despite any variability in processing conditions encountered during casting.

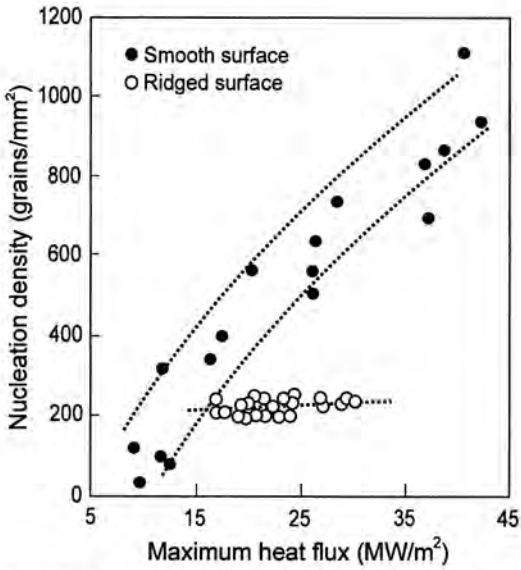

Figure 5.12. Influence of maximum heat flux on the density of nucleation sites in AISI 304 for a range of casting conditions showing the strong influence of substrate topography on nucleation density, adapted from Mukunthan *et al.* (2002).

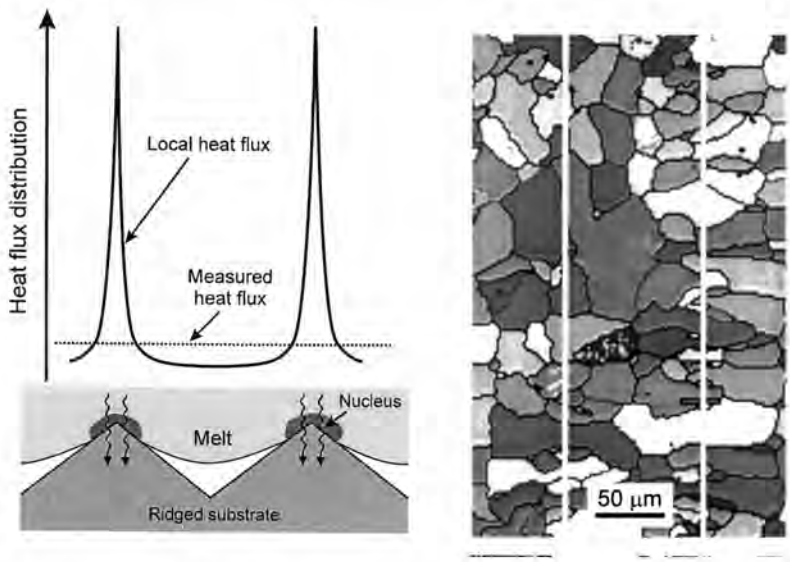

Figure 5.13. (a) Schematic diagram showing the variation in maximum interfacial heat flux during solidification onto a ridged substrate and the average value measured over a wider area. (b) EBSD micrograph of strip-cast AISI 304 showing the effect of ridges on the nucleation pattern at the surface (white lines denote melt/substrate contact regions).

5.3.2.2 Phase formation during solidification

The as-cast microstructures of austenitic stainless steels typically contain a variety of austenite-ferrite structures (Brooks and Thompson 1991). These are a result of both the solidification behaviour and subsequent solid-state transformations which are controlled by both composition and cooling rate. In multi-component Fe-Cr-Ni alloys, the $(Cr/Ni)_{eq}$ ratio is an important parameter (Table 2.4) with solidification generating either primary austenite (γ_p) or primary delta-ferrite (δ_p); the latter phase undergoes further solid-state transformations to generate a range of final microstructures (Brooks and Thompson 1991). AISI 304 stainless steel has a base composition of (wt.%) Fe-18%Cr-8%Ni ($(Cr/Ni)_{eq} = 2.25$) and a slow rate of solidification of this base alloy is expected to generate δ_p with subsequent solid-state transformation to austenite (Figure 1.6). However, other elements in the melt will alter $(Cr/Ni)_{eq}$ (§1.2.3.2) and, since the cooling rates in strip casting are high but variable (Figure 5.11), the first solidifying phase may be either γ_p or δ_p.

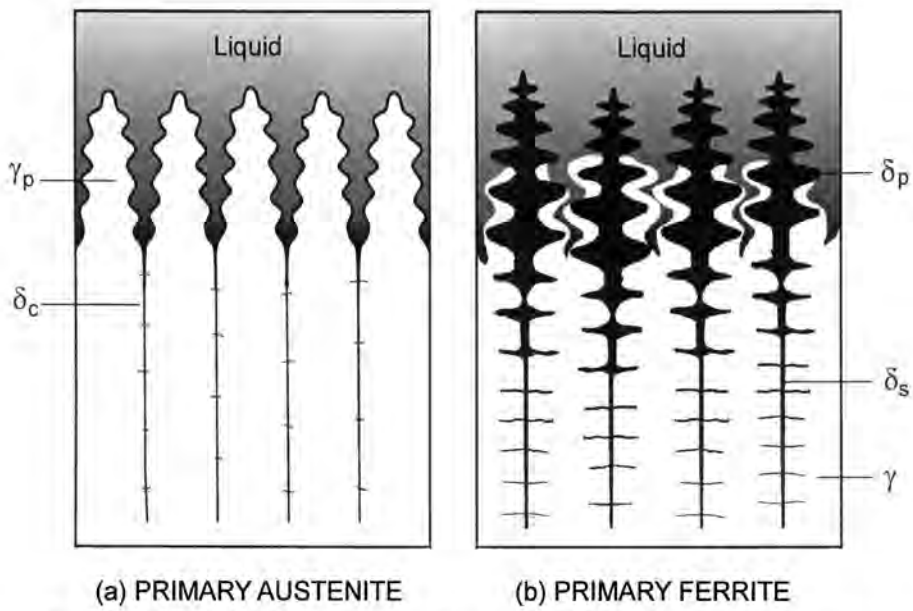

Figure 5.14. Phase formation at the advancing interface in stainless steel during dendritic solidification of: (a) primary austenite (to produce δ_c) and (b) primary delta-ferrite (to produce δ_s), adapted from Brooks and Thompson (1991).

Figure 5.14 shows schematically the transformation sequence during dendritic solidification of austenitic stainless steel for both a low and high $(Cr/Ni)_{eq}$ ratio.

For *low* $(Cr/Ni)_{eq}$ steels, γ_p is favoured with so-called *cellular* ferrite (δ_c) forming in interdendritic regions (Figure 5.14a). For *high* $(Cr/Ni)_{eq}$ steels, δ_p is expected which may subsequently transform incompletely to austenite to leave *skeletal* (δ_s) or otherwise named *vermicular* ferrite within the prior austenite grains (Figure 5.14b). Depending on the steel composition and processing conditions, other ferrite morphologies are possible (Brooks and Thompson 1991). The effect of $(Cr/Ni)_{eq}$ ratio on the solidification path of stainless steels produced by TRC was investigated by Lindenberg *et al.* (2001). The trends described in this section were generally observed and $(Cr/Ni)_{eq}$ of 1.72 (AISI 304) generated δ_p but $(Cr/Ni)_{eq}$ of 1.54 (AISI 316) generated γ_p.

The effect of solute redistribution during casting on the transformation sequence during cooling can now be summarised. If solidification commences with γ_p, Cr is rejected between the growing dendrite arms with these interdendritic regions becoming sufficiently concentrated for the eutectic reaction ($L \rightarrow \delta_c + \gamma$) to occur producing isolated globules or continuous stringers of δ_c. In contrast, the formation of δ_p results in the rejection of Ni ahead of the advancing interface which alters the local concentration of the melt for the peritectic reaction ($L + \delta_p \rightarrow \gamma$) to occur; this results in the δ_p being enveloped by γ which subsequently continues to grow. Further cooling results in the solid-state transformation of the remaining δ_p to γ but incomplete reaction will retain some skeletal ferrite within the austenite grains. Figure 1.7 illustrates the significant effect of Cr_{eq} and Ni_{eq} on the amount of delta-ferrite in the final microstructure.

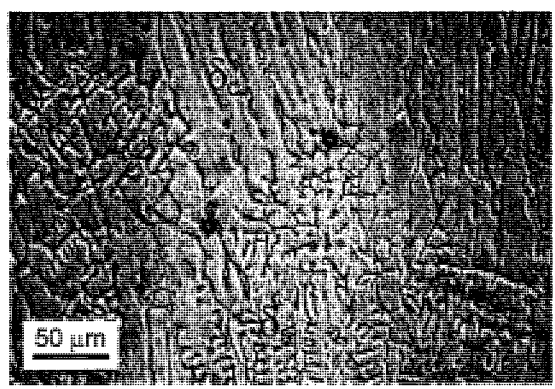

Figure 5.15. Formation of delta-ferrite in austenite in as-cast AISI 304, after Hunter and Ferry (2002d) (with kind permission of Elsevier Limited).

It is pertinent to note that γ_p may form in *high* $(Cr/Ni)_{eq}$ steels in rapid solidification processes such as electron beam or laser welding (Brooks *et al.*

1983), splat quenching (Mizukami *et al.* 1992) and strip casting (Lindenberg *et al.* 2001). For example, Mizukami *et al.* (1992) showed that splat quenching of high $(Cr/Ni)_{eq}$ steel generates cooling rates in excess of 5×10^3 K/s and the production of γ_p and δ_c. At lower cooling rates, γ_p formed at the mould surface but was replaced by δ_p as solidification proceeded with the resultant microstructure consisting of both δ_c and δ_s. An optical micrograph of such a mixed microstructure is given in Figure 5.15. It has been found that casting (and welding) may generate both skeletal and cellular ferrite within the same dendritic structure. This is believed to be associated with microsegregation during primary ferrite solidification, followed by the solidification of austenite, and finally the formation of some interdendritic cellular ferrite (Brooks and Thompson 1991).

In conventional processing of austenitic stainless steel, as-cast slabs are generally soaked for several hours at a temperature of at least 1200°C which reduces the delta-ferrite present in the microstructure to below 0.5%; hot rolling further alters the as-cast structure. In contrast, DSC produces a microstructure consisting of columnar austenite grains and a dispersion of various types of ferrite. For example, strip-cast AISI 304 often contains 2-6% delta-ferrite at room temperature with the volume fraction of this phase increasing from the surface to the core of the strip due to the increase in SDAS resulting from the decrease in cooling rate (Jeong *et al.* 1999). It was shown that the percentage of delta-ferrite depends on alloying additions and is governed by the following relation:

$$\delta(\%) = 3.3Cr_{eq} - 3.54Ni_{eq} - 18.8$$

This work is significant as an understanding of the amount of residual delta-ferrite in as-strip-cast stainless steels is important since this phase affects microstructural development during cold deformation and annealing as well as workability and corrosion resistance (chapter 6).

5.3.2.3 Segregation effects

The previous discussion has shown that solute partitioning during solidification is strongly influenced by $(Cr/Ni)_{eq}$ ratio via the formation of either γ_p or δ_p. The influence of this ratio on microsegregation was investigated by Lindenberg *et al.* (2001). The segregation profiles for AISI 304 ($(Cr/Ni)_{eq} = 1.72$) are shown in Figure 5.16a where Ni enrichment and Cr depletion are found in the interdendritic regions. In contrast, AISI 316 ($(Cr/Ni)_{eq} = 1.54$) shows the reverse trend, as well as a slightly more pronounced segregation profile (Figure 5.16b). The results shown here are similar to those found in weld deposits (Brooks and Thompson 1991). There is also an increased level of microsegregation of Mn and Si in AISI 316 which may be explained by the lower diffusivity of these elements in primary austenite relative to ferrite. It is clear that the degree of solute partitioning is determined by the formation of

either δ_p or γ_p which are influenced, in turn, by the overall steel composition and cooling rate. Nevertheless, the high solidification rates of TRC substantially refine SDAS (Figure 5.3) which should lead to a more homogeneous distribution of solute compared with conventional casting (Lindenberg *et al.* 2001).

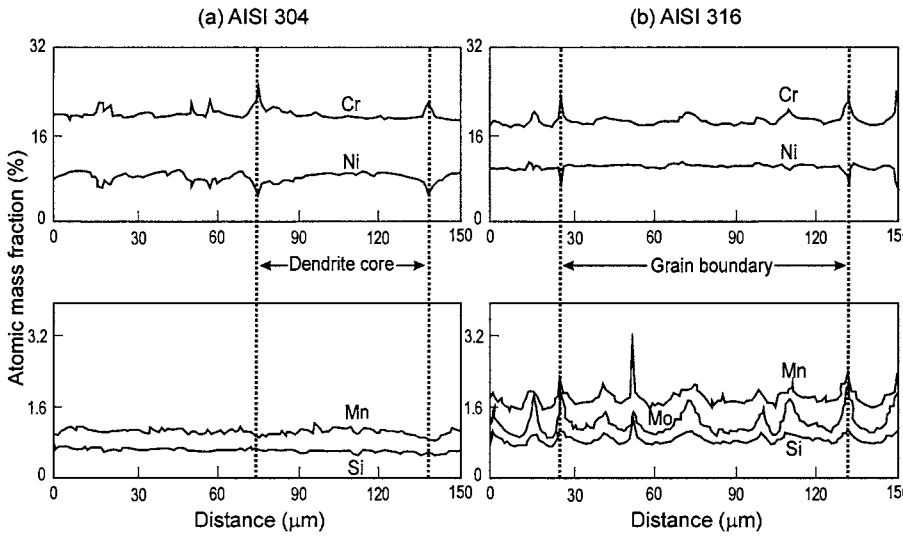

Figure 5.16. Distribution of alloying elements after TRC of stainless steels that produce either γ_p or δ_p, adapted from Lindenberg *et al.* (2001).

5.3.2.4 As-cast textures

There have been a number of studies on the solidification textures of austenitic stainless steels produced by various types of strip caster (twin roll with equal and unequal diameter rolls and single roll casters). These studies show the consistent trend of texture strengthening from the surface to the core of the strip (Takuda *et al.* 1991; Raabe 1995a,b, 1997; Hunter and Ferry 2002a). As discussed in §5.2.1, dendrites grow preferentially in the upstream direction of metal flow which is expected to produce a strong <*uvw*> fibre texture deviated by some angle towards the casting direction. In TRC, a weak surface texture is produced (Figure 5.17a) which gradually evolves into a strong TD-rotated <001> fibre texture within each solidifying shell. This produces a symmetrical distribution in orientation intensity in the core of the strip (Figure 5.17b). If solidification conditions favour the formation of a central equiaxed zone, the core of the strip will exhibit an essentially random texture separated by two <001> rotated fibre textures (Raabe 1995a).

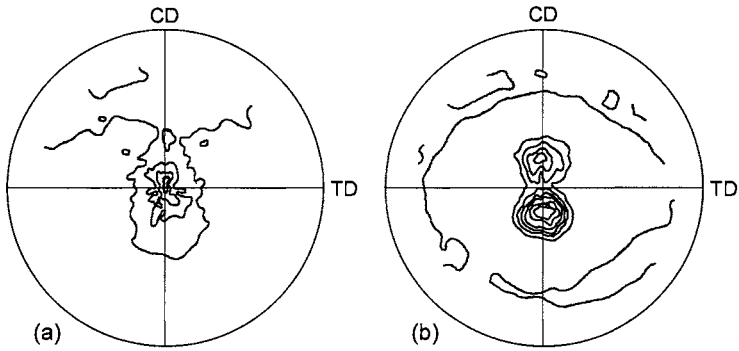

Figure 5.17. 200 pole figures showing the texture in TRC AISI 304 at: (a) the strip surface and (b) at the central region of the strip which illustrates both texture strengthening and the TD-rotated <001>//ND fibre texture produced in each shell of the strip, adapted from Takuda *et al.* (1991).

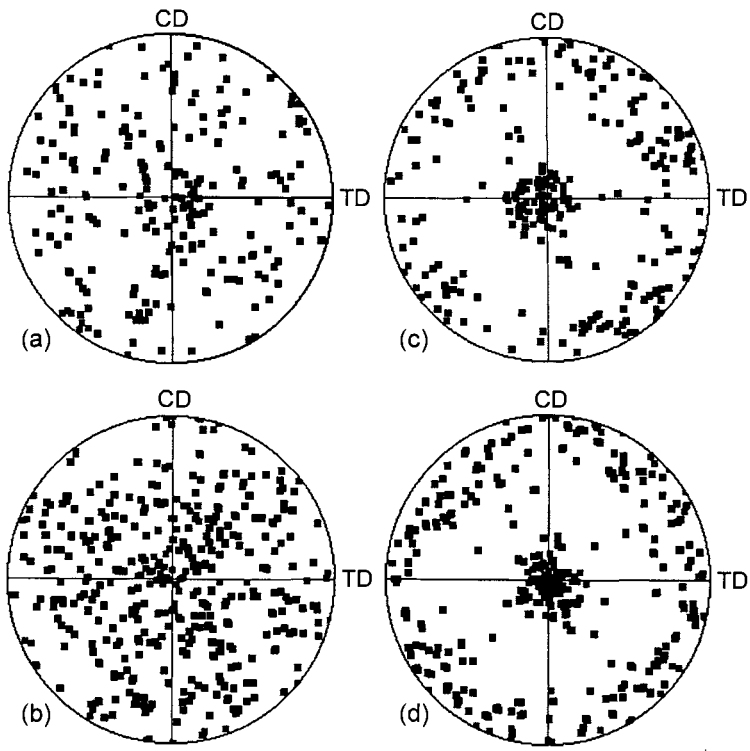

Figure 5.18. 200 pole figures of discrete EBSD measurements showing the orientation spread of grains at: (a) and (b) the substrate surface; and (c) and (d) 0.8 mm below the surface of as-cast AISI 304 strips produced from both a smooth and 20 × 180 μm ridged substrate, after Hunter and Ferry (2002a) (with kind permission of Elsevier Limited).

The influence of substrate topography on texture development in AISI 304 has been investigated in some detail by the strip casting simulator described in §A.2.2. Figure 5.18 gives 200 pole figures showing the orientation distribution of grains at the substrate surface and at 0.8 mm below the surface following solidification from a smooth and a ridged (20×180 μm) substrate. Regardless of substrate topography, grains are almost randomly-oriented at the strip surface (Figures 5.18a and b), but selective growth of <001>-oriented grains generates a strong <001> fibre texture in the core of the strip (Figures 5.18c and d).

The change in misorientation distribution of grains through the thickness of as-cast strip is demonstrated in Figure 5.19 for solidification onto a ridged copper substrate. There is a near-random distribution of misorientations at the substrate surface (Figure 5.19a), as confirmed by the superimposed theoretical distribution for randomly-oriented crystallites (McKenzie 1958). This distribution changes slightly through the strip thickness, as shown in Figure 5.19b, which is a confirmation of some texture sharpening.

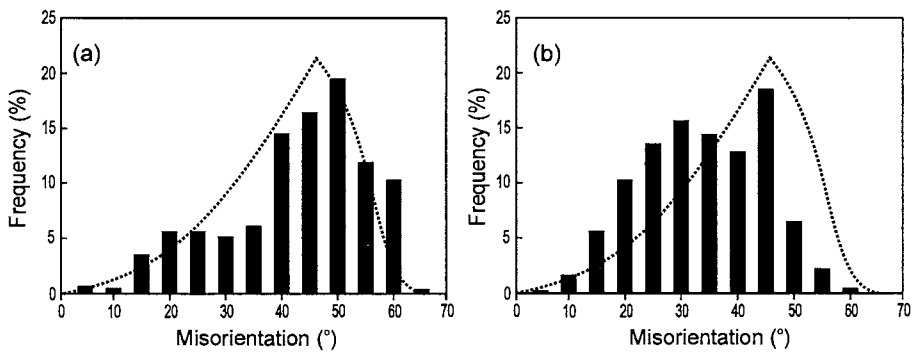

Figure 5.19. Misorientation distribution of grains at: (a) the substrate surface and (b) 0.8 mm below the surface for AISI 304 samples produced from a 20×180 μm ridged substrate (50°C melt superheat). Superimposed on the figures is the theoretical distribution for an aggregate of randomly-oriented crystallites (McKenzie 1958), after Hunter and Ferry (2002a) (with kind permission of Elsevier Limited).

5.3.3 Ferritic stainless steels

There has been limited research published on strip casting of ferritic stainless steels although this does not reduce the significance of these materials. Two major grades amenable to DSC are AISI 409 and 430 with the former leaner in Cr content and expected therefore to generate a slightly different microstructure, as indicated by the binary Fe-Cr phase diagram (Figure 1.5).

5.3.3.1 Cast structure and texture

The effect of cooling rate on microstructural development in AISI 409 (Fe-11.3Cr steel), which is expected to form primary delta-ferrite during casting (Figure 1.5), was investigated by Pryds and Huang (2000) using a wedge-shaped mould to generate cooling rates from 40 to 10^5 K/s. It was found that cooling rate has a strong influence on the grain size, morphology and size of second phase particles and the phases present in the as-cast microstructure. The results are summarised in Table 5.4 which shows the changes in phase distribution as the cooling rate is increased. In thin strip casting, cooling rates > 10^4 K/s are possible (Figure 5.3) and are expected to produce complex as-cast microstructures containing delta-ferrite, austenite, carbides and martensite.

Table 5.3. Effect of cooling rate on microstructural development in Fe-11.3%Cr alloy,* after Pryds and Huang (2000).

Position on wedge	Cooling Rate (K/s)	Phases	Morphologies	Proposed solidification path
0 – 0.5 mm	> 3700	δ, γ, Fe_3C, M	Columnar δ grains, early stage of Widmanstätten morphologies, cementite, isolated γ regions, martensite	$\delta \rightarrow L + \delta \rightarrow L + \delta + \gamma \rightarrow \delta + \gamma^* + M + Fe_3C$
0.5 – 5 mm	3700 – 368	γ, M	Columnar δ grains, martensite	$\delta \rightarrow L + \delta \rightarrow L + \delta + \gamma \rightarrow \delta + M$

* The composition (Fe-11.3Cr-0.87Mo-0.36Mn-0.77Ni-0.05C) is within the specifications of AISI 409.

Solidification experiments have been carried out on AISI 409 and 430 by TRC (Raabe *et al.* 1993; Choi *et al.* 1996) and by substrate immersion (Jonker 2000; Hunter and Ferry 2002c). These methods produce similar microstructures that are also comparable to Table 5.3 (high cooling rates) and consist of a ferritic matrix, $(Fe,Cr)_{23}C_6$ carbides and lath martensite at the grain boundaries with a higher martensite content at the chill surface of the strip. Delta-ferrite is the nucleating phase in ferritic stainless steels and, with no extensive structural changes occurring in the solid-state, an inclined <001>//ND solidification texture similar to that shown in Figure 5.18 is produced (Jonker 2000).

Solidification by TRC may also produce a weak texture in the core of the strip due to the formation of a central equiaxed zone (Raabe *et al.* 1993). Furthermore, a weak <111>//ND texture (γ-fibre) may be generated in these alloys (Raabe *et al.* 1993; Choi *et al.* 1996), indicating that some plastic deformation has occurred during casting, see *e.g.* §B.4.2.

5.3.3.2 Texture enhancement during casting

An interesting observation was made by Hunter and Ferry (2002b) of the effect of titanium on microstructural development of strip-cast AISI 409 using the strip casting simulator described in §A.2.2. The titanium level in the melt was either 0.016 or 0.15 wt.% and casting was carried out in air using a smooth copper substrate at a casting speed of 1m/s and a melt superheat of 75°C. Figure 5.20 shows EBSD micrographs of both the solidified surface (CD-TD) and ND-TD sections of Ti-free AISI 409. There are relatively few nucleation sites at the strip surface (Figure 5.20a) with coarse columnar grains growing almost parallel to ND (Figure 5.20b). In contrast, the addition of titanium results in pronounced grain refinement at the strip surface (Figure 5.20c) although the columnar morphology is retained (Figure 5.20d). The surface grain density was ~4× greater in the Ti-containing steel which indicates the marked effect of titanium on nucleation efficiency.

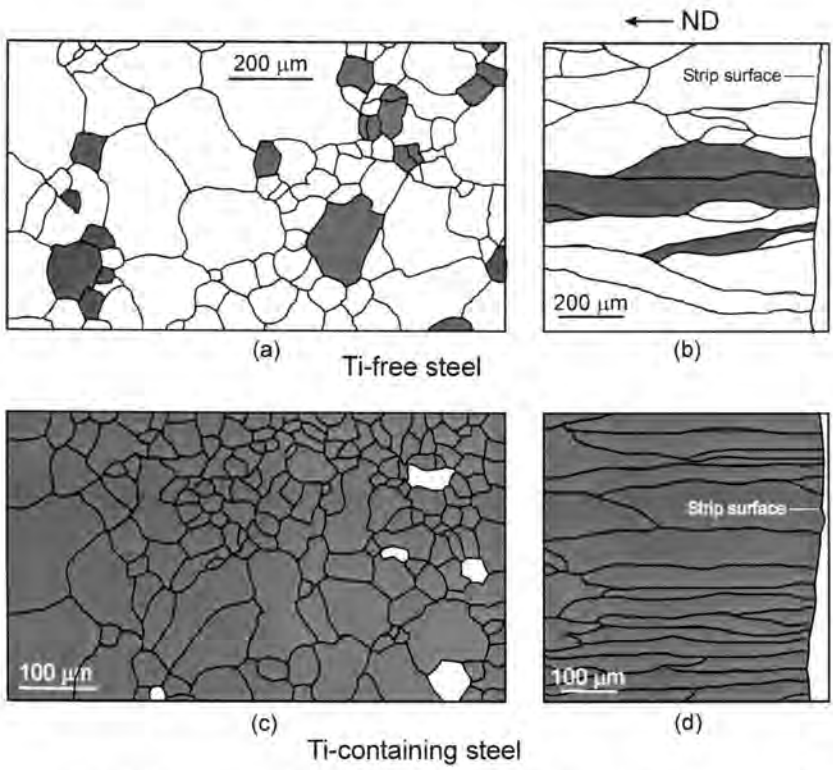

Figure 5.20. EBSD micrographs of: (a) solidified strip surface and (b) ND-TD section of the Ti-free AISI 409, and (c) solidified strip surface and (d) ND-TD section of the Ti-containing AISI 409, after Hunter and Ferry (2002b). (Gray grains are those oriented with <001> within 15° of ND) (with kind permission of The Metals, Minerals and Materials Society, USA).

The as-cast texture of the Ti-free and Ti-containing steels, respectively, are given in Figure 5.21 which shows the spread in orientation of grains at both the surface and 1 mm below the strip surface. For the Ti-free steel, grains are randomly distributed at the strip surface (Figure 5.21a) and, as expected, the preferred growth of <001>-oriented grains almost parallel to ND results in a slight sharpening of the texture (Figure 5.21c). In contrast, titanium results in a remarkably strong <001>//ND fibre texture at the strip surface (Figure 5.21b), with no significant change in texture strength during further solidification (Figure 5.21d). The degree of texture enhancement at the strip surface of the Ti-containing steel is given in Figure 5.22 which shows the area fraction of <001>-oriented grains as a function of random angular deviation from ND. The figure shows that > 95% of grains have <001> aligned within 5° of ND which is clear evidence of *oriented* nucleation.

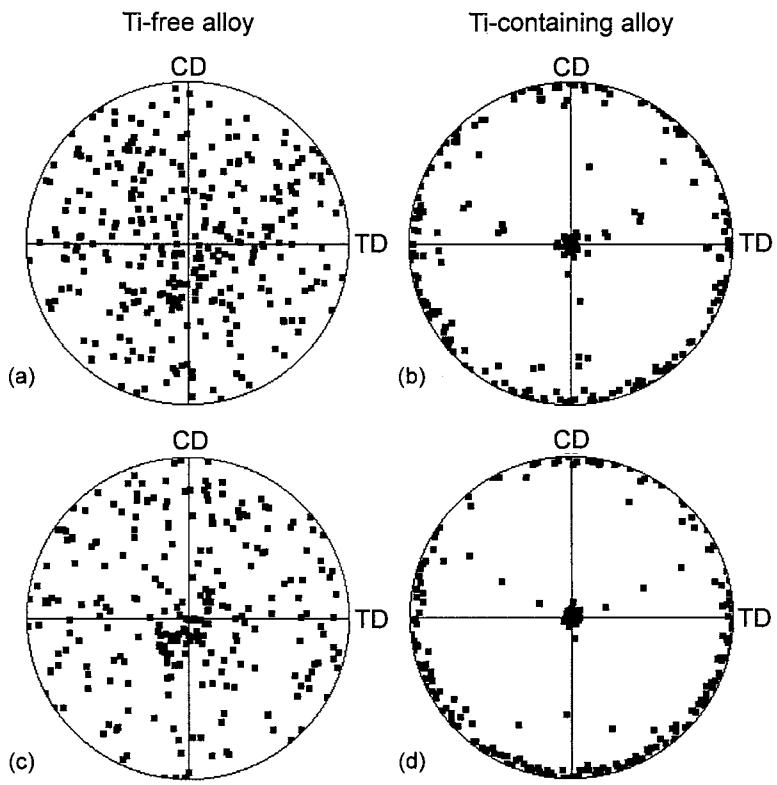

Figure 5.21. 200 pole figures of discrete EBSD measurements showing orientation spread of surface grains for (a) Ti-free and (b) Ti-containing AISI 409, and the orientation spread of grains at a distance of 1 mm below the strip surface for (c) Ti-free and (d) Ti-containing steel, after Hunter and Ferry (2002b) (with kind permission of The Metals, Minerals and Materials Society, USA).

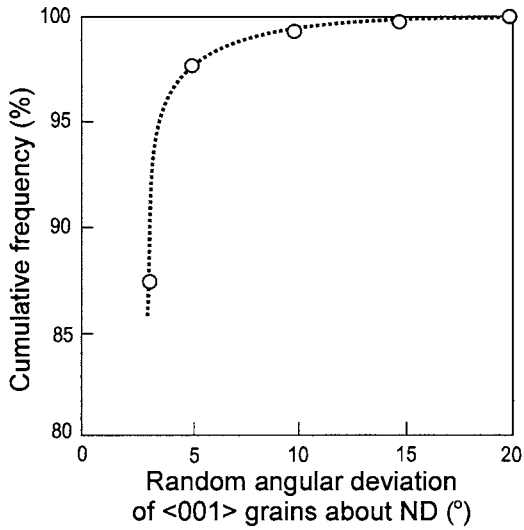

Figure 5.22. Area fraction of <001>-oriented surface grains of the as-cast Ti-containing steel strip as a function of (random) angular deviation from ND, after Hunter and Ferry (2002b) (with kind permission of The Metals, Minerals and Materials Society, USA).

There are several important factors that, in combination, are necessary for generating this remarkably sharp through-thickness <001>//ND fibre texture (Hunter and Ferry 2002b). These include: (i) the addition of titanium to the melt; (ii) casting in a nitrogen-containing atmosphere, and (iii) solidification onto a smooth substrate; textured (ridged) substrates do not generate the same effect. The combination of (i) and (ii) is expected, under certain casting conditions, to generate Ti-containing particles (Ozturk *et al.* 1995). The effect of (iii) appears to be important for nucleating ferrite grains of a pre-determined orientation with the smooth substrate surface also ensuring that heat flow is perpendicular to the substrate surface during solidification (Strezov and Herbertson 1998). It is well-known that Ti-containing compounds have similar crystallographic features to delta-ferrite and generate the following orientation relationship (Gregg and Bhadeshia 1997):

$$\{001\}_{\text{Ti-X}} \,//\, \{001\}_{\delta\text{-ferrite}}$$
$$\langle 011\rangle_{\text{Ti-X}} \,//\, \langle 001\rangle_{\delta\text{-ferrite}}$$

Figure 5.23 shows that, for the case of TiN formation, this relationship results in a very low planar disregistry (~4%) between the {001} crystallographic faces of these particles and delta-ferrite which subsequently drastically lowers the energy barrier for nucleation (see Figure 2.9). Good lattice matching is a key requirement for epitaxial growth of ferrite from inclusions of these types (Gregg

and Bhadeshia 1997; Barbaro and Krauklis 1999). The strong through-thickness <001>//ND fibre texture is therefore probably a result of inoculation, whereby Ti-rich particles must either be produced directly onto the smooth substrate (with {001} parallel to the substrate face) or form in the melt and subsequently contact the substrate at the meniscus during casting (Hunter and Ferry 2002b). These oriented Ti-rich compounds at the substrate/melt interface, together with the highly directional heat flux during solidification (using a smooth substrate) are the key to the nucleation of <001>//ND-oriented grains that subsequently grow to produce the strong through-thickness fibre texture in the as-cast strip (Figure 5.22).

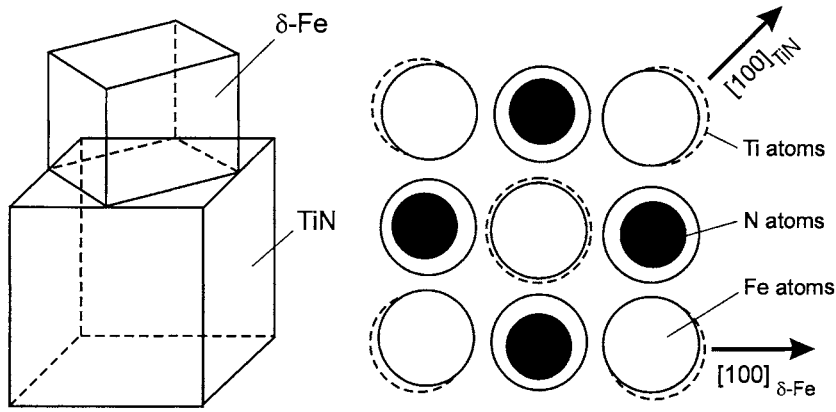

Figure 5.23. Possible crystallographic relationship between T-N and delta-ferrite showing: (a) the 45°-rotated cube-to-cube relationship and (b) details of lattice registry along coherent TiN/ferrite interface.

5.3.3.3 Comparison of texture development in strip-cast stainless steels

The transformation sequence in austenitic stainless steels during solidification is often more complex than that in ferritic stainless steels. Nevertheless, in the absence of inoculation both generate an almost random texture at the chill surface with solidification resulting in texture strengthening to produce a TD-rotated <001>//ND fibre texture. The effect of a wide range of processing conditions and alloy type on the development of <001>//ND texture during solidification is given in Figure 5.24. The results show a consistent decrease in the mean angular deviation of <001>-oriented grains from ND, $\bar{\alpha}_{<001>}$, from the surface to the core of the as-cast strips. This is a clear indication of growth selection to generate a strong rotated <001>//ND fibre texture. Figure 5.24 shows that both ferritic and austenitic stainless steels solidify in a similar manner, despite the difference in final crystal structure, the large variation in casting conditions and the different transformation sequences.

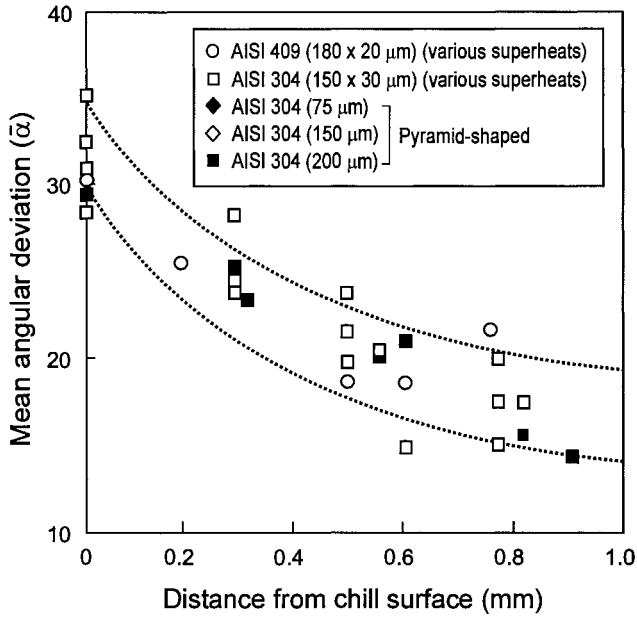

Figure 5.24. The development of <001>//ND fibre texture as a function of distance from the chill surface of a range of as-cast stainless steel strips (each data point denotes the average angular deviation of <001> from ND), after Hunter and Ferry (2002c) (with kind permission of Elsevier Limited).

5.3.4 Other ferrous alloys

Silicon iron

These alloys contain low carbon and high silicon levels to generate single-phase ferrite during solidification (§1.2.3.3). The few published studies on DSC of these alloys have shown that the solidification behaviour is consistent (Zapuskalov 1996; Takatani *et al.* 2000; Park *et al.* 2001; Landgraf *et al.* 2003). Takatani *et al.* (2000) investigated the solidification behaviour of Fe-3%Si alloy produced by TRC using electron backscatter diffraction (EBSD) measurements (§B.2). It was shown that nucleation occurs at the substrate/melt interface to produce an essentially random distribution of grains, with the gradual development of an inclined columnar grain structure in each shell of the strip (Figure 5.26a). These workers also carried out 3-D cellular automata-finite element (CAFE) modelling (§A.3.3) and confirmed that liquid metal flowing relative to the growing dendrites inevitably results in their growth being inclined towards the casting direction to generate a symmetrical TD-rotated <001>//ND fibre texture (Figure 5.26b). The grain structure and texture of twin roll cast silicon iron are therefore similar to that produced in stainless steel (§§5.3.2-5.3.3).

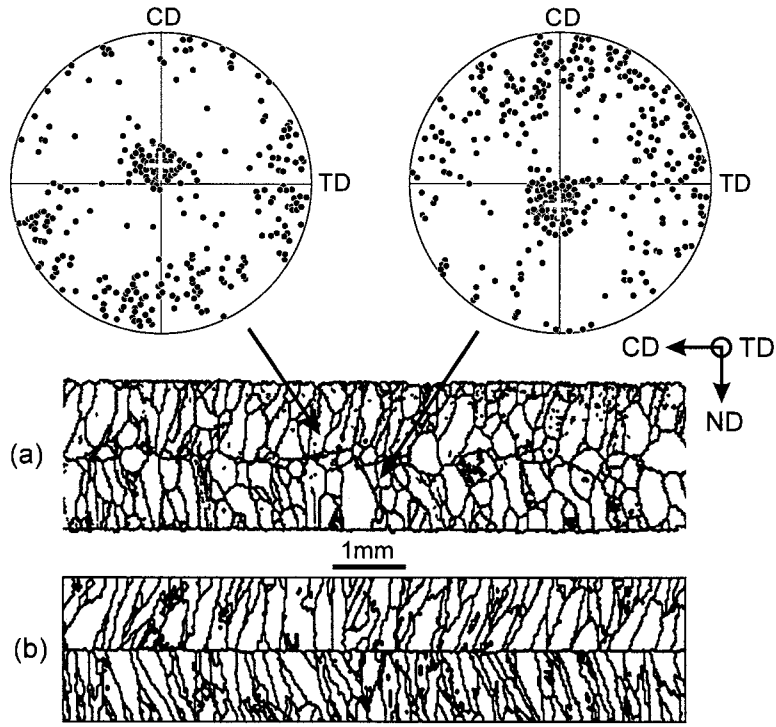

Figure 5.26. (a) Experimental and (b) CAFE simulated columnar grain structures in twin roll cast Fe-3%Si alloy. The 001 pole figures shown in (a) are generated from EBSD line scans at ¾ thickness of each shell of the as-cast strip, after Takatani *et al.* (2000) (with kind permission of Elsevier Limited).

Invar (Fe-Ni) alloys

These alloys contain ~ 35 wt.% Ni and are therefore expected to be austenitic at room temperature (Figure 1.7). They are usually produced by ingot casting process but Park *et al.* (2002) have demonstrated that twin roll casting into thin-gauge sheet is possible and problems of segregation, oxidation and cracking that plague alloys produced by conventional processing routes are alleviated. There are, however, considerable differences in the microstructure and texture as TRC generates a non-uniform structure consisting of a randomly oriented chill zone at the strip surfaces with most of the strip comprising of the classic columnar microstructure with dendrite deflection angles of up to 30° in the casting direction (Park *et al.* 2002). Therefore, the TD-rotated {100}<*uvw*> texture is again produced throughout much of the strip (see *e.g.* Figure 5.26). It has been reported that a weak copper-type rolling texture may develop in the core of the strip if solidification occurs ahead of the roll nip thereby causing a

limited amount of plane strain deformation as the strip passes through the roll bite of the caster (Park *et al.* 2002).

Melt-spun soft magnetic alloys

Iron alloys are also processed by the more severe melt-spinning processes outlined in §3.3.4 to produce far-from-equilibrium microstructures exhibiting a range of novel properties. Recent developments in alloy design can produce alloys with an amorphous matrix, a nanocrystalline matrix or a nanocrystalline phase embedded in an amorphous matrix (Jiles 2003). These structures are generally highly complex and contain various alloying elements in order to generate the amorphous phase.

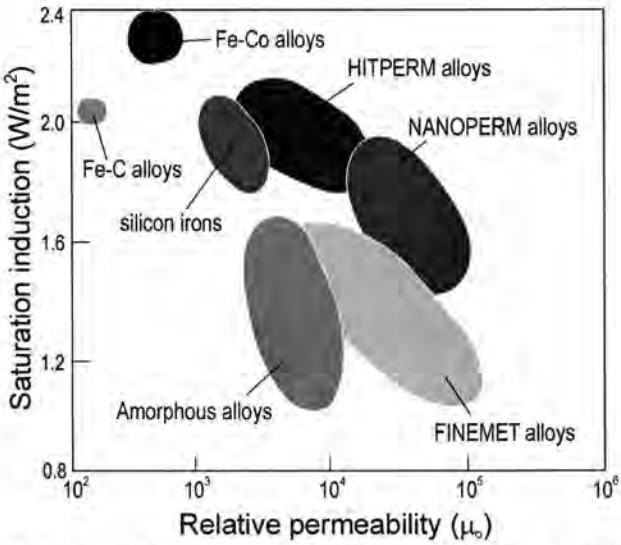

Figure 5.27. Estimated relationship between permeability and saturation induction for some melt-spun soft magnetic iron alloys, after Ferry (2005) (with kind permission of Elsevier Limited).

There are a number of commercially-available melt-spun iron alloys that possess an excellent combination of soft magnetic properties: high permeability, low coercivity and low hysteresis losses (McHenry and Laughlin 2000; Jiles 2003). These include FINEMET™ ($Fe_{73.5}Si_{13.5}B_9Nb_3Cu_1$), NANOPERM™ ($Fe_{88}Zr_7B_4Cu_1$) and HITPERM™ ($Fe_{44}Co_{44}Zr_7B_4Cu_1$) which are produced by melt-spinning and crystallization annealing to produce a nanocrystalline structure. Compared with more conventional iron alloys, these materials have very high permeabilities and large inductions (Figure 5.27).

5.4 Strip-cast non-ferrous alloys

5.4.1 Aluminium alloys

A range of aluminium alloy sheet products has been produced for over five decades using: (i) wheel and band casters; (ii) Hazelett-type twin-band casters (Figure 3.9); (iii) block chill casters (Figure 3.10), and (iv) twin roll casters (Figure 3.12c). In TRC, the range is restricted to low solute alloys; higher solute alloys are very difficult to cast due to their affinity for hydrogen, poor oxidation resistance and wide freezing range (see §3.3.1.3). Nevertheless, these alloys are readily produced by thick-strip-casting (Hazelett-type) processes and the recently-developed 4-Hi TRC process shown in Figure 3.18. Improvements in caster design at FATA Hunter Inc., USA and Pechiney, France also allows a wider range of alloys to be cast by TRC. There are other emerging casting techniques to produce clad composites (Figure 3.13) and combinations of casting and forming operations to generate higher formability strip (see e.g. §6.7.1.3).

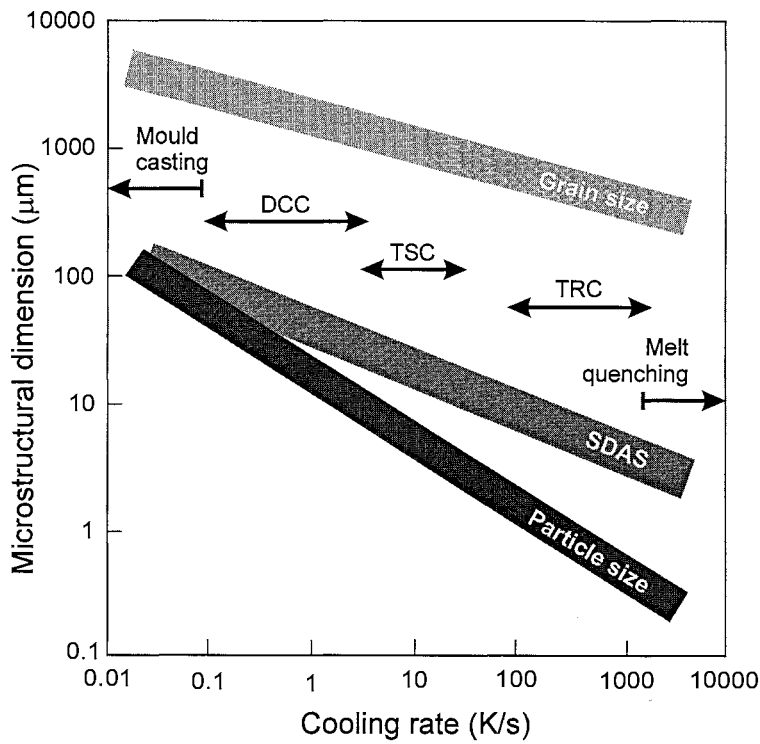

Figure 5.28. The influence of cooling rate on as-cast grain size, secondary dendrite arm spacing (SDAS) and size of intermetallic particles in a range of commercial aluminium alloys, adapted from Furrer (1989) and Merchant *et al.* (1989).

It is pertinent to note that the commercially significant process of TRC of aluminium is substantially different to that of steel (see chapter 4). For example, the former almost always incorporates a horizontal or near-horizontal molten metal feed system, steel rolls are used rather than copper and there is a roll lubricating system. There is also substantial deformation of the strip during casting (§4.4.2). The combination of these factors generates different as-cast microstructures in aluminium strip compared with steel. The influence of various processing variables on heat transfer and strip deformation during casting was discussed in chapter 4, which is essential for understanding the important metallurgical characteristics of as-cast aluminium strip: grain structure and texture; intermetallic and precipitate distribution; supersaturation and segregation.

5.4.1.1 General microstructure

The influence of cooling rate on a range of important microstructural parameters is summarised in Figure 5.28 for various Al alloys. Superimposed on the figure is the casting procedure that generates a particular range of cooling rate. It is clear that TRC and melt-quenching processes can refine the microstructure by several orders of magnitude compared with DCC and static casting processes. There is a consistent trend in microstructural refinement with increasing cooling rate. For example, TRC generates a fine grain size (30-100 μm), SDAS (3-8 μm) and intermetallic particle size (0.1-1 μm).

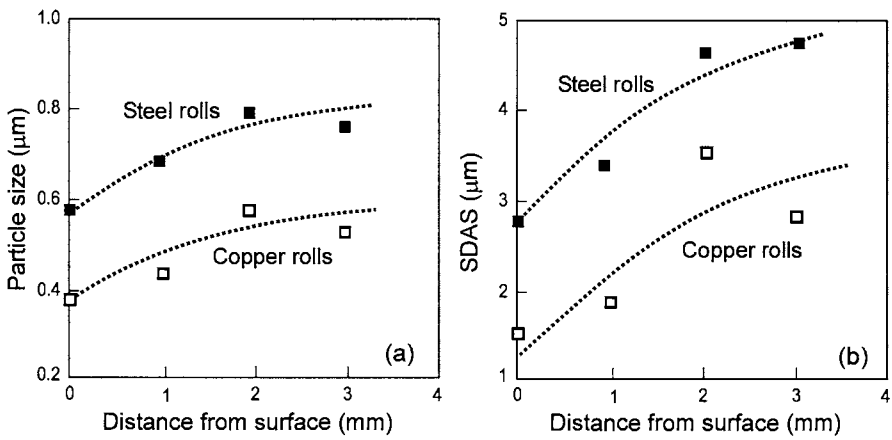

Figure 5.29. Effect of roll material and cooling rate on (a) intermetallic particle size and (b) SDAS for TRC Al-Mn alloy strip, after Nes and Slevolden (1979).

The effect of roll material in TRC on intermetallic size and SDAS is shown in Figure 5.29. For copper rolls, the cooling rates are up to 100× more rapid than

steel rolls which results in considerable refinement of these microstructural parameters. The figure also demonstrates the expected coarsening from the surface to the core of the strip. In addition to microstructural refinement, the high solidification rates often associated with strip casting of aluminium alloys favours the formation of metastable phases, reduces the volume fraction of phases, increases the solubility of alloying elements and, hence, promotes supersaturation (Merchant *et al.* 1989). An example of the increase in solubility of iron in aluminium is given in Figure 5.30 which shows that the greatest increase in supersaturation with increasing cooling rate occurs for low iron additions and results in almost complete solubility at rates in excess of 100 K/s; such rates are readily achieveable by TRC.

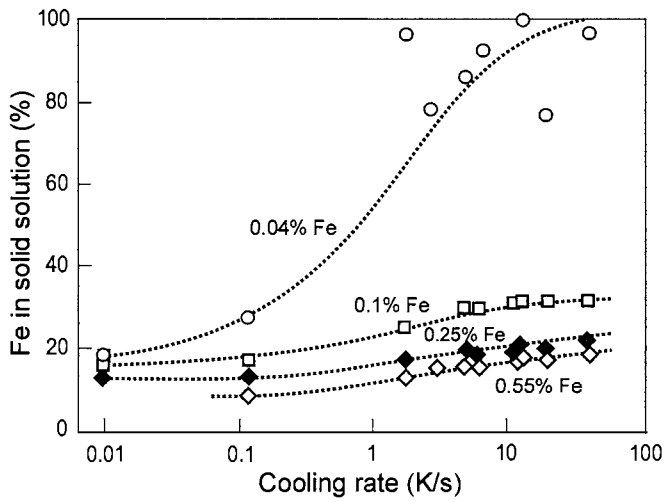

Figure 5.30. Effect of cooling rate during solidification on the degree of supersaturation of iron in aluminium for a range of binary Al-Fe alloys, after Miki *et al.* (1975) (with kind permission of Japan Institute of Light Metals).

A notable difference between twin roll casters and belt/block casters is the generation, in the latter, of a very deep liquid metal sump (Figure 4.17) and moderate cooling rates (Figure 5.28). Hence, deep-sump casters produce only a slightly different microstructure to that of DCC, whereas the high cooling rates associated with TRC result in considerable microstructural refinement (Figure 5.31). It is useful to note that TRC also produces a thinner gauge strip compared with belt casting which tends to restrict the downstream processing window and makes the large freezing range alloys (high Mg, Zn and Cu levels) more difficult to cast. This is significant as AA2XXX, 5XXX and 7XXX alloys are used in a wide range of important structural applications (§1.3.1). Nevertheless, a number of developments are currently underway in attempts to strip-cast these alloys (§3.3.3).

5.4.1.2 Grain and particle morphology

Aluminium alloys are often inoculated with a suitable grain refiner prior to casting (§2.2.1.3). During casting of thick-gauge Al alloy strip (belt and block cast), the heat flow at the melt/substrate interface is not extreme and the use of an effective grain refiner will generate only a slightly elongated or even an equiaxed grain structure. However, casting may not involve grain refinement and the structure, particularly for TRC of thin-gauge strip, is often characterised by columnar grains that nucleate at the roll surfaces and grow inward in a highly-oriented manner but with a slight inclination towards the casting direction. Roll-bite deformation is also a common feature of TRC of aluminium due to the large tip setback associated with the process (§4.4.2). Figure 5.32 shows that deformation in the as-cast strip further rotates the columnar grains and generates substantial shearing at the strip surface. It is pertinent to note that the very high strains needed to produce the microstructure in Figure 5.32b are not normally encountered in TRC (Merchant *et al.* 1989).

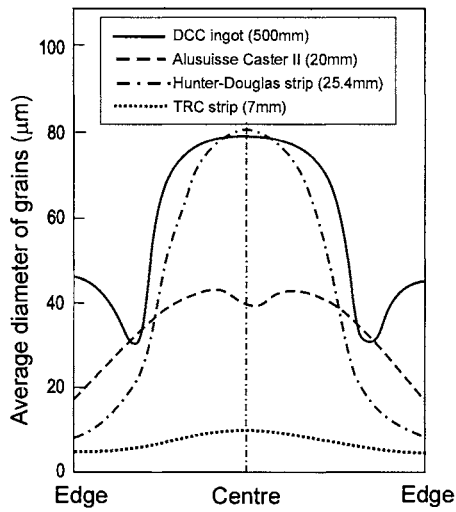

Figure 5.31. Diagram showing the through thickness distribution of dendrite arm spacing for DCC, belt/block and TRC, adapted from Buxmann and Gold (1982).

An additional influence of a large tip setback in TRC is the further refinement of the intermetallic particles produced by casting. Figure 5.33 shows that increasing tip setback refines the particle size and produces a narrower size distribution which is a result of substantial roll-bite deformation of the fully solidified strip. A large deformation also produces a more homogeneous distribution of very fine particles at the strip surface which was found to improve the formability of the strip (Naess 1989).

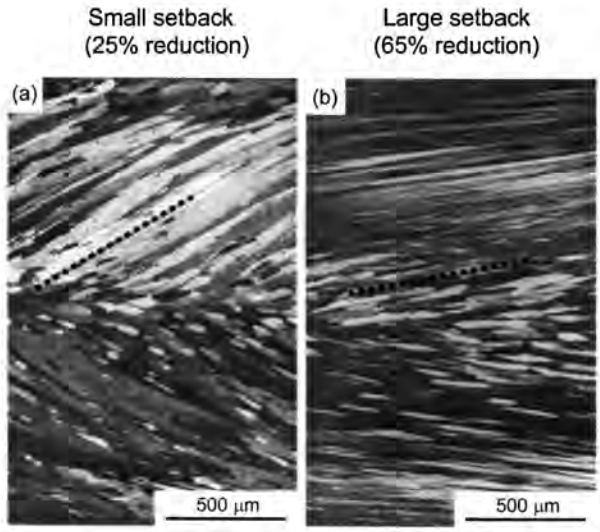

Figure 5.32. Effect of degree of setback in twin roll casting of an aluminium alloy on grain rotation due to hot deformation, after Naess (1989) (with kind permission of The Metals, Minerals and Materials Society, USA).

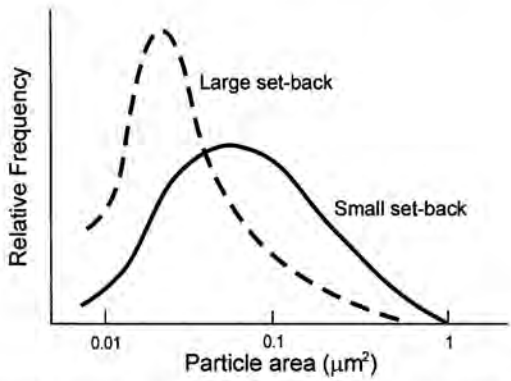

Figure 5.33. Particle size distribution in twin roll cast AA 3103 for small and large setback, after Naess (1989) (with kind permission of The Metals, Minerals and Materials Society, USA).

The origin of the particle refinement shown in Figure 5.33 was discussed by Naess (1989) and is shown schematically in Figure 5.34. During TRC, the total roll-bite deformation is a combination of plane strain compression and a shear component (Gras *et al.* 2005). For a small tip setback, the major strain component is compression whereas a higher setback results in substantial shear deformation, particularly in the outer regions of the strip. In the absence of substantial shear, the particle distribution is attributed to simple stretching in

the rolling direction (Figure 5.34a) whereas a large shear leads to heterogeneous deformation which tends to break up the grains into blocks in order to retain continuity in the material (Figure 5.34b). Hence, the particles produced by casting will be sheared in the thickness direction to produce a finer size and narrower size distribution, Figure 5.33.

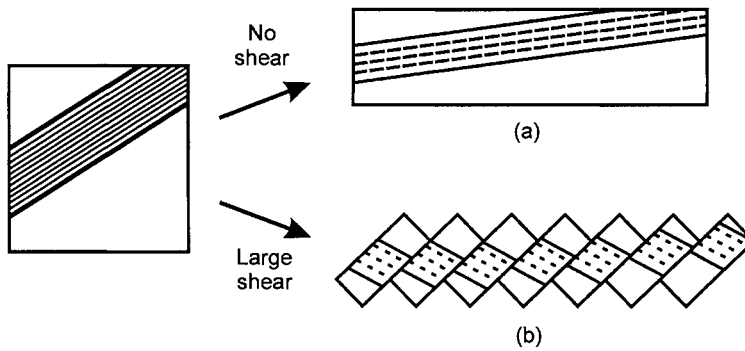

Figure 5.34. Schematic illustration of the influence of inhomogeneous deformation during TRC on the disintegration of the as-cast structure, after Andersson and Tibballs (1989) (with kind permission of The Metals, Minerals and Materials Society, USA).

5.4.1.3 Texture development

While <001> dendritic growth is expected in most fcc metals (Table 2.2), there are numerous reports of other growth morphologies in a range of Al and Cu alloys (Henry *et al.* 1998). During semi-continuous casting, these alloys often develop grains of feathery morphology that are not composed of regular <001> dendrites but <011> primary dendrite arms in which the higher order <011> arms are twin related. During directional solidification, these grains undergo a selection mechanism similar to that observed for <001> dendritic grains that eventually generates a strong <011> fibre texture. Other exotic dendritic morphologies have been observed including untwinned <011> dendrites that form under high thermal gradients and solidification rate and other degenerate feathery morphologies with <011> primary arms and <001> secondary arms (Henry *et al.* 1998).

In light of the different growth behaviour of dendrites associated with rapidly-cooled Al alloys, strip-cast textures in Al alloys may be different to those produced in other cubic metals. One of the first reliable studies of of texture development in twin roll casting was carried out by Radonjic *et al.* (1982) on AA1050. In the strip interior (Figure 5.35a) there is a well-developed texture with maximum intensity reasonably close to the {110}<112> (brass) components. The brass texture is expected for grains of feathery morphology if the aforementioned <011> growth selection operates during directional

solidification. It is pertinent to note, for the same alloy, that the addition of a grain refiner during casting generates an essentially equiaxed microstructure with a strong {111}<*uvw*> and weaker {100}<011> texture component (Figure 5.35b).

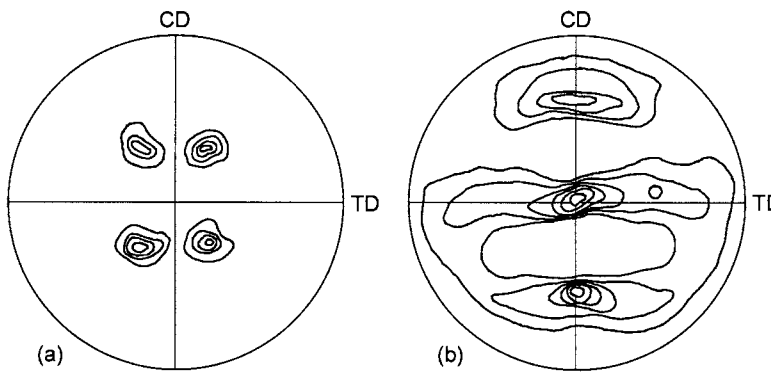

Figure 5.35. 111 pole figures of twin roll cast AA 1050 showing the texture at the strip interior for: (a) no grain refinement, and (b) grain refinement, adapted from Radonjic *et al.* (1982).

Andersson and Tibballs (1989) carried out a detailed study of the effect of roll bite deformation in a 7 mm gauge Al alloy produced by twin roll casting and found that the degree of tip setback has a notable influence on texture development (Figure 5.36). A small tip setback produced a TD-rotated {110}<001> (Goss) texture just below the strip surface (Figures 5.36a(i) and 5.36a(ii)) which developed into a strong texture in the core of the strip with maximum intensities near {110}<112> (Figure 5.36a(iii)). In contrast, the additional deformation caused by a large tip setback resulted in substantial shear in the surface regions of the strip (see Figure 5.32). Despite the slightly higher true strain (ε ~0.3), shearing generated a substantially different texture in these regions with peak intensities close to {100} < 011 > and {111} < *uvw* > (Figure 5.36b(i)). These texture components are similar to that observed by Radonjic *et al.* (1982) (Figure 3.35b). With increasing distance from the strip surface, there was a gradual change to a TD-rotated {110}<001> texture (Figure 5.36b(ii)) and, finally, to a classic {112}<111> (Cu-type) rolling texture at the core of the strip due to the substantial plane strain deformation in this region (Figure 5.36b(iii)).

The results shown in Figure 5.36 are largely consistent with the recent work of Gras *et al.* (2005) whereby AA3105 was twin roll cast to 2 mm gauge strip and the texture examined both in the vicinity of the surface and core of the strip. Taking their casting parameters (roll diameter of 400 mm and feed metal tip setback of 35-55 mm), and estimating a sump depth of ~10 mm at a casting

speed of 4.5 m/min (Figure 4.19), Eq. 4.1 predicts a rolling strain ranging from 44 to 72% reduction during casting. Figure 5.37 shows $\varphi_2 = 0°$ and $\varphi_2 = 45°$ sections in Euler space of the texture at the surface and core of the as-cast strip. At the strip surface, the notable texture components are $\{100\} < 011 >$ and $\{111\} < uvw >$ which are similar to the texture components in cold rolled bcc metals (Figure 6.11). These texture components are also similar to that shown in Figures 5.35b and 5.36b(i). In contrast, the core of the as-cast strip has developed a weak Cu-type rolling texture (β-fibre), similar to that shown in Figure 5.36b(iii).

Overall, microstructure and texture development in strip-cast aluminium alloys differs from that in ferrous alloys due to the different growth morphologies of the dendrites, possible grain refinement by inoculation in aluminium and the large deformations associated with casting. The type and strength of the texture of as-cast aluminium strip is expected to have a strong influence on the texture following cold rolling and annealing (§6.6.3.3), which in turn affects the formability of the material (§6.7.1.3).

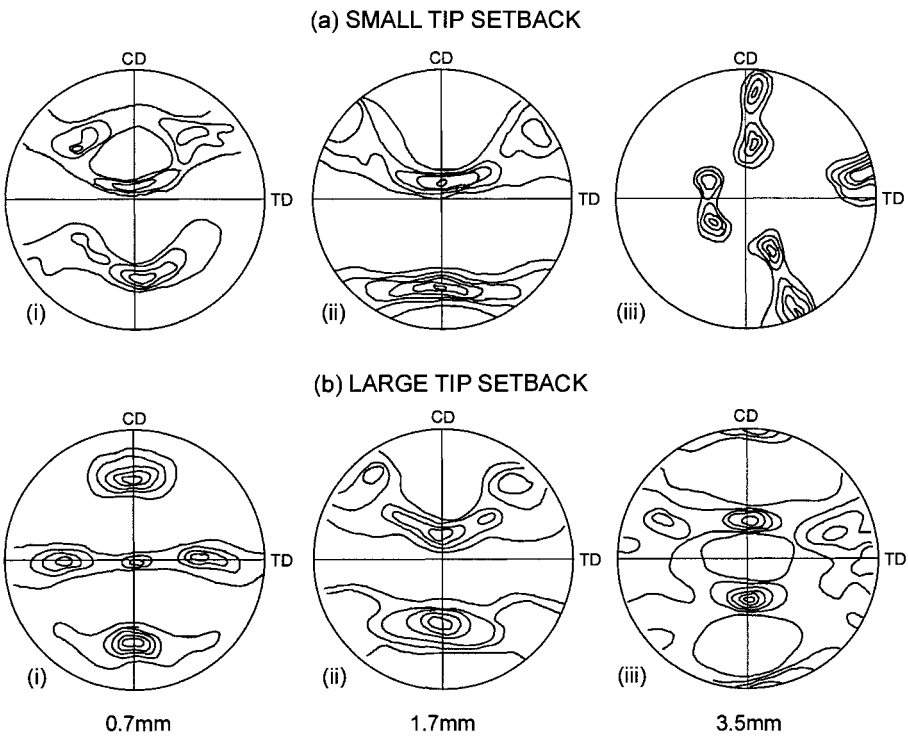

Figure 5.36. 111 pole figures for various depths for a medium strength Al-alloy strip produced by twin roll casting for: (a) small and (b) large tip setback, adapted from Andersson and Tibballs (1989).

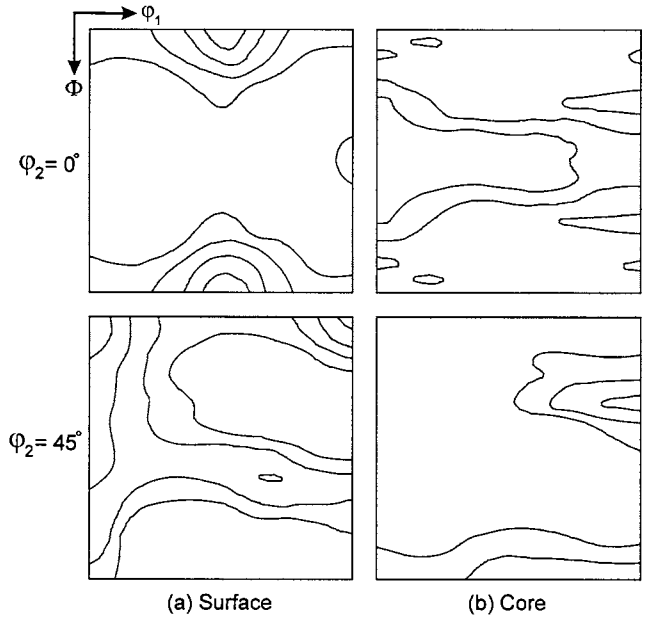

Figure 5.37. $\varphi_2 = 0°$ and 45° sections of Euler space showing the texture at the: (a) surface and (b) core of twin roll cast AA3105 strip (1, 2, 4, 7 × random), adapted from Gras *et al.* (2005) (with kind permission of Elsevier Limited).

5.4.1.4 Segregation effects

In aluminium alloys, the mode of strip casting, solidification conditions and alloy type are amongst the most important factors that need to be controlled to minimise a range of metallurgically derived defects such as macro- and microsegregation, centre-line segregation, porosity, level lines, edge cracks, surface bleeds and spangles (Merchant *et al.* 1989; Lockyer *et al.* 1996). Segregation is a major internal defect associated with TRC of Al alloys. It has been investigated extensively by Hunt and co-workers and is described in detail in §4.6.1.

5.4.2 Magnesium alloys

Magnesium alloy sheet products are usually produced by a similar process to aluminium alloys, i.e.: (i) direct chill casting into slabs of up to 30 mm x 1000 mm x 2000 mm; (ii) homogenisation at about 480°C, and (iii) hot and cold rolling with various annealing stages throughout the process. Compared with aluminium and iron alloys, strip casting of magnesium has not developed beyond the pilot plant stage but the process is certainly feasible and likely to be an important processing route in the near future due to the need to reduce the manufacturing cost of magnesium sheet.

To transform DSC into a commercial process for magnesium, the various challenges outlined in Table 3.3 must be met. For example, the process must be capable of producing strip from a wide range of alloys with different thickness (especially below 4 mm) with the technology used in TRC of Al alloys. The process must have a high success rate at the commencement of a casting run, a safe termination and use existing infrastructure for secondary processing such as rolling and annealing operations. However, modification of the composition of conventional alloys may be necessary due to the wide solidification range of commercially-available Mg-Al-Zn alloys (Figure 1.12).

5.4.2.1 Cast structure and texture

Like aluminium, Mg has no allotropic transformations and the degree of structural refinement possible during casting is limited. Hence, the cast structure can be altered only by further secondary processing such as homogenisation, hot or cold rolling and annealing. At the time of writing, there is very little published on the development of microstructure and properties of Mg alloys produced by DSC (Park *et al.* 2003, 2005; Davey *et al.* 2004; Liang and Cowley 2004; Watari *et al.* 2004a,b). Liang and Cowley (2004) have reported promising results for TRC of the commercially-significant Mg alloys AZ31, AZ61, AM60 and AZ91 (Table 2.8). A range of thicknesses down to 2.5 mm was produced at cooling rates comparable to those found in aluminium alloys. A similar refinement in microstructural parameters was generated including a reduction in the size of both intermetallic particles and grains (Figure 5.28) and an increase in solubility (Figure 5.30). These factors resulted in a significant improvement in the mechanical properties of the as-cast strips.

Nucleation and growth of grains during DSC of magnesium is expected to occur in a manner similar to that in the alloys discussed previously. Although there is very little documentation, the mode of casting (belts or rolls) and casting parameters such as casting velocity, melt superheat and substrate topography are all likely to affect the as-cast microstructure. Grain refiners may also be added during casting to generate a finer, more equiaxed grain structure. In the absence of inoculants, the as-cast grain structure of twin roll cast Mg alloys is either equiaxed or columnar with the latter often producing a central equiaxed zone. Park and co-workers (2003) have shown that a high melt superheat favours dendritic growth in AZ31 (low freezing range alloy) which subsequently generated a structure consisting of columnar grains inclined in the direction of casting and an equiaxed zone at the core of the strip. However, they observed a fully equiaxed structure in AZ91 which was attributed to the wide freezing range of this alloy and the low melt superheat.

Figure 5.38 shows an increase in SDAS with distance below the strip surface of twin roll cast AZ31 and AZ91 alloys; this behaviour is characteristic of all alloys produced by DSC. It can also be seen that AZ31 developed a finer dendrite arm spacing than AZ91; this may be a result of the different melt superheats used

during casting (118°C for AZ31 and 52°C for AZ91). The higher melt superheat in AZ31 is expected to result in a high cooling rate and will result in refinement of the dendrite arm spacing (see Eq. 2.37). The narrower freezing range (ΔT_o) in AZ31 compared with AZ91 is also expected to contribute to the SDAS refinement, as predicted by Eq. 2.36.

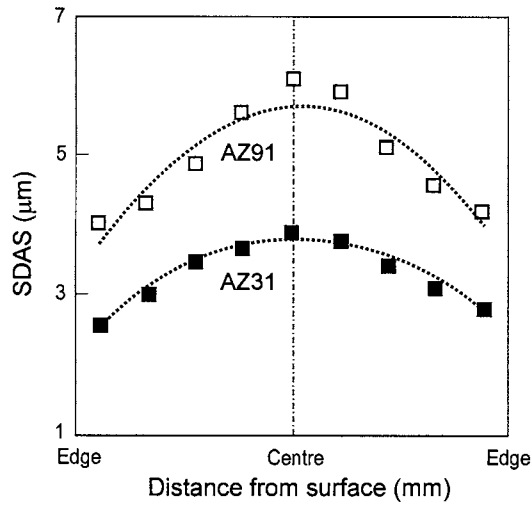

Figure 5.38. SDAS as a function of distance from the as-cast surface of twin roll cast magnesium alloys AZ31 and AZ91, after Park *et al.* (2003) (with kind permission of Trans Tech Publishers).

Unlike cubic metals, the preferred dendritic growth directions in hexagonal metals are $<10\bar{1}0>$, (Table 2.2); this will generate different solidification textures. As in other alloys, the alloy type, casting velocity together with other casting variables (tip setback, roll diameter, final gauge, melt superheat etc.) will affect the final microstructure and texture of as-cast magnesium strip. Nevertheless, there are no reports in the open literature of texture development in strip-cast magnesium alloys and further work is needed.

5.4.2.2 Potential for downstream processing

The tendency to form coarse columnar grains in strip cast magnesium may result in problems with workability if the material is to be further processed by rolling or fabricated into a final shape. A coarse columnar structure can be replaced by a more equiaxed structure by inoculation of the melt, a standard practise in DCC of these alloys, or by lowering the casting temperature. However, there are several potential problems with inoculation in DSC such as nozzle clogging and upstream nucleation. Inoculation may not be necessary if DSC can generate a refined columnar structure or a fully equiaxed structure.

5.4.3 Copper alloys

Direct chill casting of copper alloys into ingots is a more favourable process than static casting for the subsequent production of thin strip products. The advantages of DCC have been described in §3.2.1.1, and include improved casting plant productivity, better quality ingots and greater flexibility in cast ingot sizes. Nevertheless, some alloys, such as phosphor-bronzes (§1.3.4), are difficult to produce by DCC and conventional hot rolling due to problems with hot shortness (Renschen and Lewis 1989). Strip casting of highly alloyed copper alloys tends to avoid the problems associated with hot shortness and segregation as the process is capable of replacing hot rolling with cold rolling and annealing to produce the final strip product (Carlsson *et al.* 1990).

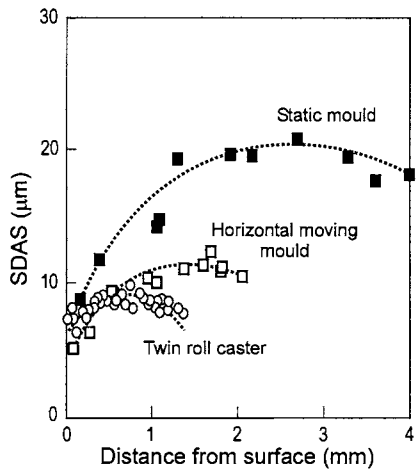

Figure 5.39. SDAS as a function of distance from the as-cast surface of Cu-Sn-Ni alloy produced by different casting routes, after Es-Sadiqi et al. (1989) (with kind permission of The Metals, Minerals and Materials Society, USA).

Some possible casting configurations for DSC of copper alloys are given in Figures 3.14 and 3.22, respectively, but TRC to produce thin gauge strip is also feasible (Kim *et al.* 2005). As for other alloys, the very short local solidification times associated with TRC produce a finer SDAS compared with other casting processes (Figure 5.39) where spacings < ~10 μm are produced throughout the strip. The microstructures of copper alloys generated by DSC are similar to that produced in other cubic metals with relatively coarse columnar grains extending at an angle from the surface to the core of the strip and either a central equiaxed zone or fully equiaxed microstructure may develop for various alloys under certain casting conditions (Carlsson *et al.* 1990; Kim *et al.* 2005). The as-cast textures of these alloys are also characterised by a TD-rotated <001>//ND fibre texture.

5.4.4 Other non-ferrous alloys

Titanium alloys

The processing of titanium foils by conventional ingot metallurgy involves casting ingots, hot forging into billets followed by several hot rolling, heat treatment and surface grinding sequences to produce plate or sheet that is suitable for cold rolling into thin-gauge sheet (Collings 1984). Gapsar *et al.* (1991, 1994) and Weaver and Garmestani (1998) have successfully cast commercial purity titanium, titanium alloys and Ti-base intermetallics into strip form using a single-roll casting technique termed melt overflow rapid solidification technology (MORST). These workers noted several potential advantages of DSC over conventional ingot metallurgy routes such as improved purity, increased chemical homogeneity and a reduction in processing losses resulting in reduced overall costs.

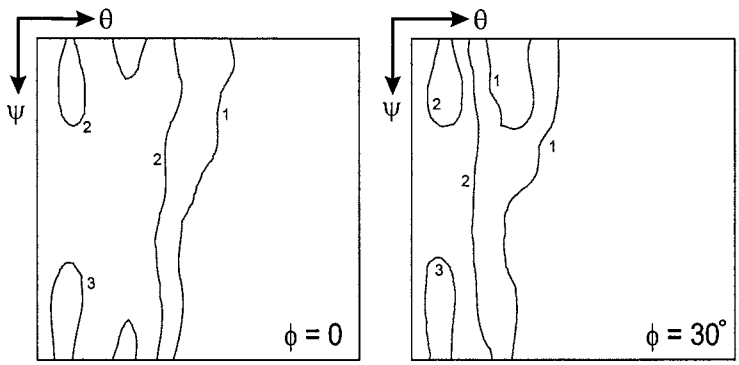

Figure 5.40. Solidification texture of commercial purity titanium strip produced by single roll casting, after Weaver and Garmestani (1998) (with kind permission of Elsevier Limited).

As-cast strip of 0.5 mm thickness and 100 mm width has been produced by the MORST process. The as-cast foils were found to exhibit microstructures, textures and mechanical properties comparable to those produced by conventional routes. The as-cast microstructure of a commercial purity titanium alloy consists largely of large columnar grains originating from the surface of the roll with grain diameters of 35 to 200 μm and some equiaxed grains forming near the free surface of the strip. Due to the allotropic transformation in titanium (§1.3.3), the structure transforms on cooling to a mixture of acicular and serrated α phases. The solidification texture produced on the wheel surface of the caster is shown in Figure 5.40 as $\phi = 0°$ and $\phi = 30°$ sections in Euler space (Roe notation). The final texture is very weak and consists mainly of a TD-rotated $\{11\bar{2}0\}$//ND texture but there is evidence of a tube of orientations from $(\bar{1}010)[1\bar{2}10]$ to $(\bar{1}018)[0\bar{1}10]$. This weak texture is

likely to be a result of the $\beta \rightarrow \alpha$ transformation that occurs in commercial purity titanium during cooling.

Nickel alloys

The limited work on DSC of nickel alloys indicates that the most popular process is TRC (Yukumoto and Yamane 1995; Dalle *et al.* 2003). For example, Yukumoto and Yamane (1995) twin roll cast Ni-8%Fe-17%Cr (Inconel 606) to produce strip of 0.2 to 0.8 mm thickness and 250 to 500 mm width for the production of overlay welding hoops. In order to suppress precipitation and other unwanted structural changes after casting, the strip was subjected to water spray cooling at 300-350°C/s on leaving the caster and coiled at ~400°C. The resulting microstructure is similar to that of other strip-cast alloys that do not undergo any allotropic transformations and consists of a fine columnar grain structure almost parallel to ND. These grains exhibit a characteristic as-cast dendritic structure with SDAS varying from 2 to 3.5 μm at the surface to the core of the strip.

Palladium alloys

Korzekwa and co-workers (1992) carried out melt spinning experiments on Pd-Ni alloy using the apparatus shown in Figure 3.16a. The results are similar to those found for DSC of other cubic metals that do not undergo further solid-state transformations. The melt-spun ribbons exhibited a near-random texture at the strip surface that intensified due to the orientation selection mechanism described in §2.2.2.6 to develop the classic TD-rotated <001> fibre texture with dendrites inclined ~20° from ND (Figure 5.41).

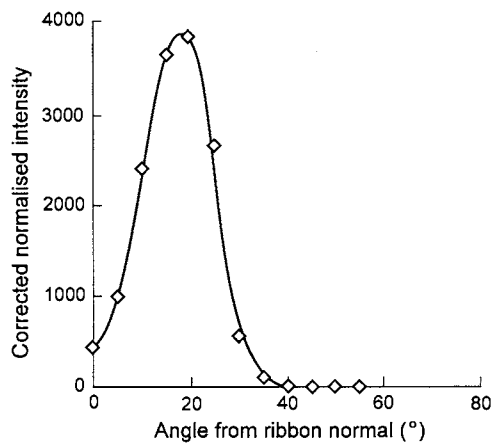

Figure 5.41. Intensity distribution of grains rotated about TD towards CD in a melt-spun Pd-Ni alloy, after Rollett and Wright (1998) (with kind permission of Cambridge University Press, UK).